



Experimental Investigation on Physical and Mechanical Properties of Granite Subjected to Cyclic Heating and Liquid Nitrogen Cooling

Guan Rong^{1,2} · Song Sha^{1,2} · Bowen Li^{1,2} · Zhiheng Chen^{1,2} · Ziyang Zhang^{1,2}

Received: 9 July 2020 / Accepted: 25 January 2021 / Published online: 13 February 2021
© The Author(s), under exclusive licence to Springer-Verlag GmbH, AT part of Springer Nature 2021

Abstract

Cyclic liquid nitrogen (LN₂) fracturing is an innovative technology for reservoir stimulation with great potential in geothermal energy exploitation. Understanding of the mechanical responses of high-temperature rock to repetitive LN₂ cooling at the laboratory scale is of great relevance to facilitate the field application of cyclic LN₂ fracturing. In this work, granite samples were subjected to 0–24 heating–cooling cycles in two manners (i.e., slow heating to 300 °C followed by air cooling or LN₂ cooling), and subsequent a series of laboratory tests with the aim of investigating the damage characteristics and mechanisms of rock samples after different heating–cooling cycles. The results concluded that increasing the number of cycles aggravates the internal structural damage of granite, which further deteriorates its physico-mechanical properties. Compared with air cooling, the cold shock effect of LN₂ is more capable of facilitating the growth of microcracks within the rock, thereby inducing a more severe initial damage to granite sample. However, the damage of granite is prominent only in the first few cycles, and basically no longer intensified after more than about 12 cycles. This is related to the fact that the increase in micro-defects provides more space for thermal deformations of minerals and reduces the level of thermal stress within the rock. The results in this study are instructive for evaluating the effectiveness of cryogenic fracturing and determining the reasonable number of LN₂ fracturing during reservoir stimulation.

Keywords Geothermal energy · LN₂ fracturing · Rapid cooling · Heating–cooling cycles · Physical and mechanical properties

List of Symbols

| | |
|------------------|---------------------------------------|
| M | Mass (g) |
| ρ | Density (g/cm ³) |
| n | Porosity (%) |
| V_p | P-wave velocity (m/s) |
| V | Bulk volume (cm ³) |
| V_v | Pore volume (cm ³) |
| M_{sat} | Saturated-surface-dry mass (g) |
| M_s | Grain mass (g) |
| ρ_w | Density of water (g/cm ³) |

| | |
|-----------------|--|
| σ_t | Brazilian tensile strength (MPa) |
| P | Failure load (N) |
| d | Diameter (mm) |
| t | Thickness (mm) |
| σ_{cc} | Crack closure stress (MPa) |
| σ_{ci} | Crack initiation stress (MPa) |
| σ_{cd} | Crack damage stress (MPa) |
| σ_p | Peak strength (MPa) |
| E | Young's modulus (GPa) |
| ε_p | Failure strain |
| $D(I)$ | Damage variable |
| I_N | Physico-mechanical properties of rock after N cycles |
| I_0 | Physico-mechanical properties of intact rock |
| I_N | Physico-mechanical properties of rock after N cycles |
| σ_{ts} | Thermal stress (MPa) |
| $\Delta\alpha$ | Difference of thermal expansion coefficient (/°C) |
| ΔT | Temperature difference (°C) |
| R^2 | Correlation coefficient |

✉ Song Sha
songsha@whu.edu.cn

✉ Bowen Li
libowen@whu.edu.cn

¹ State Key Laboratory of Water Resources and Hydropower Engineering Science, Wuhan University, Wuhan 430072, China

² Key Laboratory of Rock Mechanics in Hydraulic Structural Engineering, Ministry of Education, Wuhan University, Wuhan 430072, China

1 Introduction

The growing energy demand and the worsening environmental pollution are two major challenges facing the world today. Exploring renewable and environmentally friendly energy resource is an effective way to address such issues. In recent decades, a special interest has been devoted to hot dry rock (HDR) geothermal energy due to its great potential in industrial and residential applications (Wyborn 2005). In general, the HDR reservoirs are composed of the compact granite or other crystalline rocks at depths in the order of 5–6 km, with a temperature variation of 150–500 °C (Potter et al. 1974; Gallup 2009; Breede et al. 2013). At present, the exploitation of HDR geothermal energy is mainly by virtue of Enhanced Geothermal System (EGS), which circularly pumps the working fluid through the doublet well configurations to achieve heat exchange (Olasolo et al. 2016; Barla 2017; Rybach 2014). Due to the ultra-low permeability of reservoir matrices, the permeability enhancement technology has to be taken to improve the thermodynamic efficiency and productivity of EGSs.

In terms of the current field applications, hydraulic fracturing is a common means to enhance the permeability of unconventional reservoirs. It is reported that more than 90% of shale gas wells and 70% of oil wells in the world are required to carry out large-scale hydraulic fracturing for effective exploitation (Brannon 2010). However, due to the high reliance on water, hydraulic fracturing cannot avoid the disadvantages of waste of water resources, clay hydration swelling and environmental pollution (Sinal and Lancaster 1987; Jackson et al. 2013; Bahrami et al. 2012; Boudet et al. 2014). To solve these problems, a novel waterless fracturing technology, liquid nitrogen (LN₂) fracturing, is proposed and gradually developed during the past decades (Li et al. 2016). As the fracturing fluid, LN₂ is a colorless, tasteless, and inert liquid with an extremely low temperature of about -196 °C at normal atmospheric pressure (Jacobsen et al. 1986). Unlike the traditional hydraulic fracturing processes, LN₂ fracturing does not cause the issues associated with the use of water-based fracturing fluids, as well as has the advantages of cleanliness, low price and high construction safety (Wang et al. 2016).

LN₂ fracturing is first proposed by Shouldice (1964) to assist drilling and completion operations. In the 1990s, it was also successfully applied in coalbed methane and shale gas extraction (McDaniel et al. 1997; Grundmann et al. 1998), which verifies the feasibility of cryogenic fracturing with LN₂ for reservoir stimulation. In recent years, a great deal of experimental works has been conducted to investigate the effect of LN₂ freezing on the

physico-mechanical properties and microstructure of rocks at room temperature (Finnie et al. 1979; Inada and Yokota 1984; McDaniel et al. 1997; Cai et al. 2014a, b, 2015; Qin et al. 2016, 2017; Yang et al. 2017b; Han et al. 2018; Wu et al. 2018; Gao et al. 2018). The results from these studies revealed that the cryogenic LN₂ had outstanding performance in enhancing the connectivity of pore structure, promoting the expansion of thermal cracks, and reducing mechanical strength of rocks. To systematically study the damage characteristics and mechanisms of cryogenic fracturing, Cha et al. (2017) developed a laboratory system for cryogenic fracturing under true-triaxial loading conditions, which can perform LN₂ fracturing on 20 cm cubic rock blocks. On this basis, Alqatahni et al. (2016) conducted a series of LN₂ cryogenic fracturing experiments on concrete, sandstone and shale samples under different stress conditions. The results showed that the fracturing effect could be improved by increasing the injection of LN₂, and the expansion direction of fracturing fractures was obviously controlled by the magnitude and anisotropy of confining pressure. Wu et al. (2019) performed a transient fluid-thermo-structural coupling simulation to investigate the cooling effect during LN₂ jet impingement. According to the results, LN₂ jet induced higher tensile and shear stresses in rocks, thus could achieve better rock-breaking performances than water jet. Qin et al. (2018a, b) conducted a comparative study on the heat and mass transfer process and fracture propagation behaviors of coal samples under single and cyclic LN₂ injection conditions. They pointed out that the fracturing efficiency of the cyclic LN₂ injection is far higher than that of single LN₂ injection. From their results, the damage of coal sample after a single LN₂ injection treatment was mainly concentrated in the area adjacent to the injection tube, while cyclic injection method notably expanded damage area and form a propagated fracture network in rocks.

In comparison, cryogenic fracturing is a relatively novel fracturing technology that has not been well investigated in either laboratory or field. According to the literature review, most previous studies were mainly focused on the oil and gas reservoir rocks at room temperature (e.g., coal, shale and sandstone), and few researches have been done on high-temperature crystalline rocks in HDR reservoirs. In addition, although LN₂ has been demonstrated to have great potential for reservoir stimulation, the feasibility and effectiveness of cyclic LN₂ fracturing in HDR reservoir are still unclear. The aim of this paper is to investigate the influence of cyclic heating—LN₂ cooling on the physico-mechanical behaviors of granite. The granite samples were subjected to 0–24 heating–cooling cycles in two ways, i.e., slow heating to 300 °C followed by air cooling or LN₂ cooling. A comparative analysis was conducted to studied the variations in the physico-mechanical behavior of granite after different

heating–cooling cycles. In addition, the development of microcracks within the sample was evaluated based on acoustic emission (AE) monitoring and microscopic observations. Meanwhile, the damage evolution and mechanisms of the granite under cyclic heating–cooling cycles were revealed. It is expected that the results of the present study would provide some new insights for extracting geothermal energy assisted by cyclic LN₂ fracturing.

2 Materials and Methodology

2.1 Rock Sample Characterization

Granite is an igneous crystalline rock that form by crystallization of certain slow-cooling magma invading the upper formation. It is reported that more than 60% of the EGSs are performed on granite formations (Potter et al. 1974; Breede et al. 2013; Vidal and Genter 2018). Therefore, the granite is selected in this study to carry out relevant experiments. The rock material was collected from a mine located in Macheng City, Hubei Province, China. The mineral composition of the granite is obtained by X-ray diffraction analysis, as presented in Table 1. It is seen that the main mineral compositions of the granite sample are feldspathic minerals and quartz. Figure 1a presents the microstructure of the granite observed from thin slice. From the figure, the internal structure of the rock is intact in natural state, and the minerals are tightly bound together.

Table 1 Mineral composition of the granite sample

| Mi (%) | Ab (%) | Qtz (%) | Mu (%) | Chl (%) |
|--------|--------|---------|--------|---------|
| 39.56 | 30.97 | 20.45 | 7.23 | 1.79 |

Mi microcline, *Ab* albite, *Qtz* quartz, *Mu* muscovite, *Chl* chlorite

To conduct uniaxial compression tests and Brazilian splitting tests, the cylindrical samples (Φ50×100 mm) and disk samples (Φ50×25 mm) were prepared in strict accordance with the specifications recommended by ISRM (Ulusay and Hudson 2007), as shown in Fig. 1b. The ends of all samples were carefully grind and polished to ensure flatness at both ends of less than 0.02 mm. Visual inspection reveals that the granite sample has a uniform texture and no visible defects. Prior to conduct thermal treatments, the physico-mechanical properties of granite samples subjected to 7 days of air drying were measured and tested, and the main results are summarized in Table 2.

2.2 Cyclic Heating–Cooling Treatment and Nomenclature

The heating processes of rock samples were carried out in a SX3-10-12 box-type resistance furnace. Since the temperature of geothermal reservoirs currently exploited is generally lower than 350 °C (Bertani 2005; Breede et al. 2013), 300 °C was selected as the predetermined thermal treatment temperature in this study. A slow heating rate of 5 °C/min was employed during heating to ensure that the microcracks within the rock are not a result of thermal shock (Dwivedi et al. 2008; Yavuz et al. 2010). After attaining the target

Table 2 Summary of physico-mechanical properties of granite sample before treatment (mean ± standard deviation)

| Physico-mechanical properties | Average values |
|---|----------------|
| Density ρ (g/cm ³) | 2.61 ± 0.02 |
| Porosity n (%) | 0.82 ± 0.01 |
| P-wave velocity V_p (m/s) | 4430 ± 26 |
| Young’s modulus E (GPa) | 70.11 ± 3.47 |
| Brazilian tensile strength BTS (MPa) | 5.42 ± 0.18 |
| Uniaxial compressive strength UCS (MPa) | 160.37 ± 6.18 |

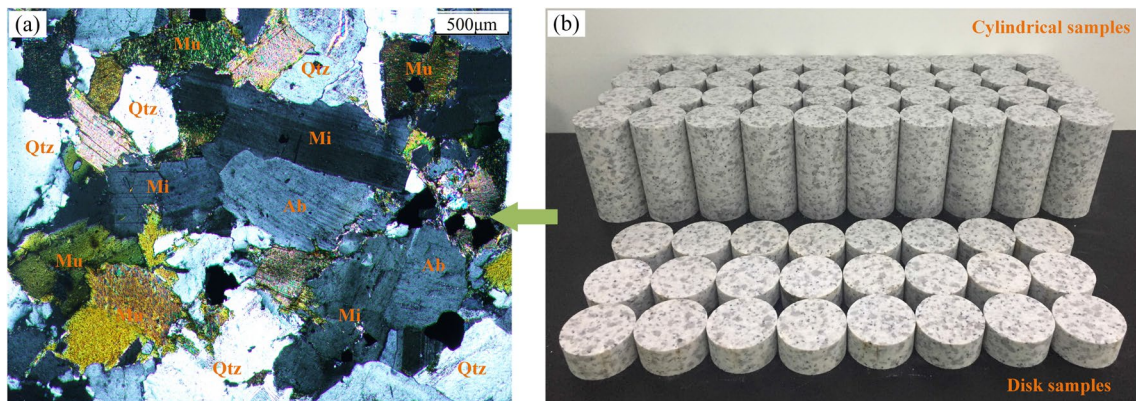


Fig. 1 a Microstructure of granite observed from the thin slice, and b photograph of the prepared standard cylindrical and disk samples

temperature, the rock samples were held thermostatically in the furnace for 4 h to sufficiently heat. Subsequently, the samples were cooled to room temperature in two different ways: (1) rapid cooling by LN₂ immersion (i.e., LN₂ cooling), and (2) slow cooling in the atmospheric environment (i.e., air cooling). At this point, one heating–cooling cycle was complete. A total of seven heating–cooling cycles were set in the present study, i.e., 0 (no heating–cooling treatment), 1, 3, 6, 12, 18 and 24. Figure 2 shows the schematic of these two types of heating–cooling cycles. To improve the reliability of the experimental results, three repeated experiment were carried out on the cylindrical and disk samples under each cycle cooling condition. For the sake of convenience, the granite sample after LN₂ cooling is referred to as “LG” in this study, and the sample after air cooling is referred to as “AG”.

2.3 Instrument and Test Procedure

Prior to mechanical testing, the physical properties of the sample, such as mass (M), bulk volume (V), porosity (n) and P-wave velocity (V_p), were first measured before heating and after cooling. The M and size (i.e., height and diameter) of the rock were measured separately using electronic balance and vernier caliper, both with an accuracy of 0.01. To reduce the measurement errors, the height and diameter were measured three times at different positions of the sample and then averaged. The V and density (ρ) of the granite can be easily obtained based on the above measurement results.

As per ISRM-recommended method (Ulusay and Hudson 2007), n of the granite sample was measured utilizing a ZK-270 vacuum saturation device. First, the rock sample was immersed in water under the vacuum pressure of 0.1 MPa for 24 h to reach saturation. After drying surface, the sample was weighted to determine the saturated-surface-dry mass. Thereafter, the saturated sample was dried at 105 °C for

24 h by virtue of an air-dry oven, then weighted again to obtain the grain mass. The porosity of the specimen can be determined as

$$n = \frac{100V_v}{V} \% \quad (1)$$

where V_v is the pore volume, and V is the bulk volume. V_v can be calculated by the following equation:

$$V_v = \frac{M_{\text{sat}} - M_s}{\rho_w} \quad (2)$$

where M_{sat} is the saturated-surface-dry mass, M_s is the grain mass, and ρ_w is the density of water.

V_p is highly sensitive to the growth of micro-defects within the tested material (Homandtienne and Troalen, 1984; Chaki et al. 2008), therefore, it can be used to qualitatively evaluate the level of microstructural damage of the samples after different heating–cooling treatments. In this study, V_p of the granite sample was measured utilizing an RSM-SY5(T) acoustic detector based on the ultrasonic pulse transmission technique. The sample was placed between the two transducers, and a constant pressure was applied to bring them into close contact. In the meantime, the interfaces between the sample and the transducers were coated with a layer of Vaseline film to ensure energy effectively transfer. Under each heating–cooling cycle, V_p measurement was performed on three cylindrical samples, and repeated five times for each sample. The average V_p was then calculated as the final measurement result.

In this study, the mechanical properties of the granite sample were tested employing a hydraulic servo-controlled compression system (TAW-3000), which has a maximum loading capacity of 3000 kN and an accuracy of 0.01% (see Fig. 3a). The Brazilian splitting method was utilized to determine the tensile strength of rock sample because of its

Fig. 2 Schematic o of cyclic heating–cooling process

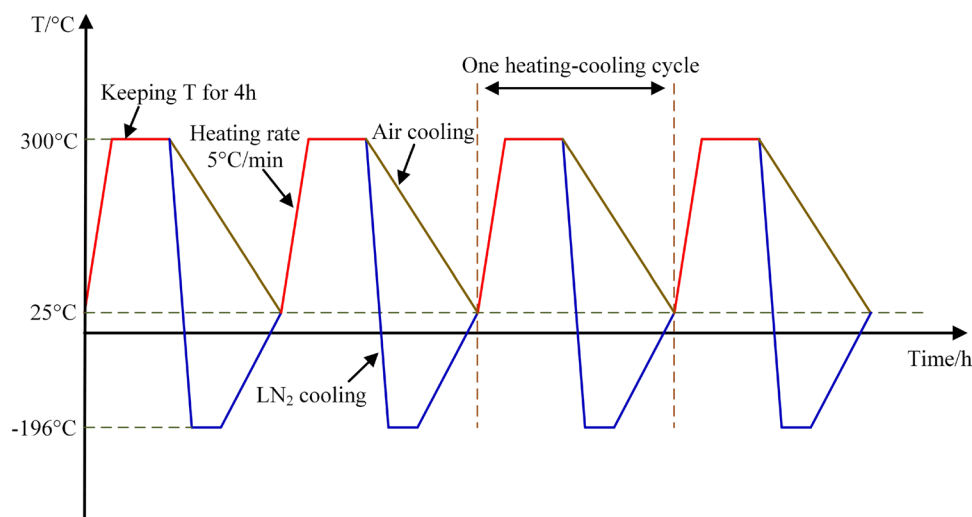
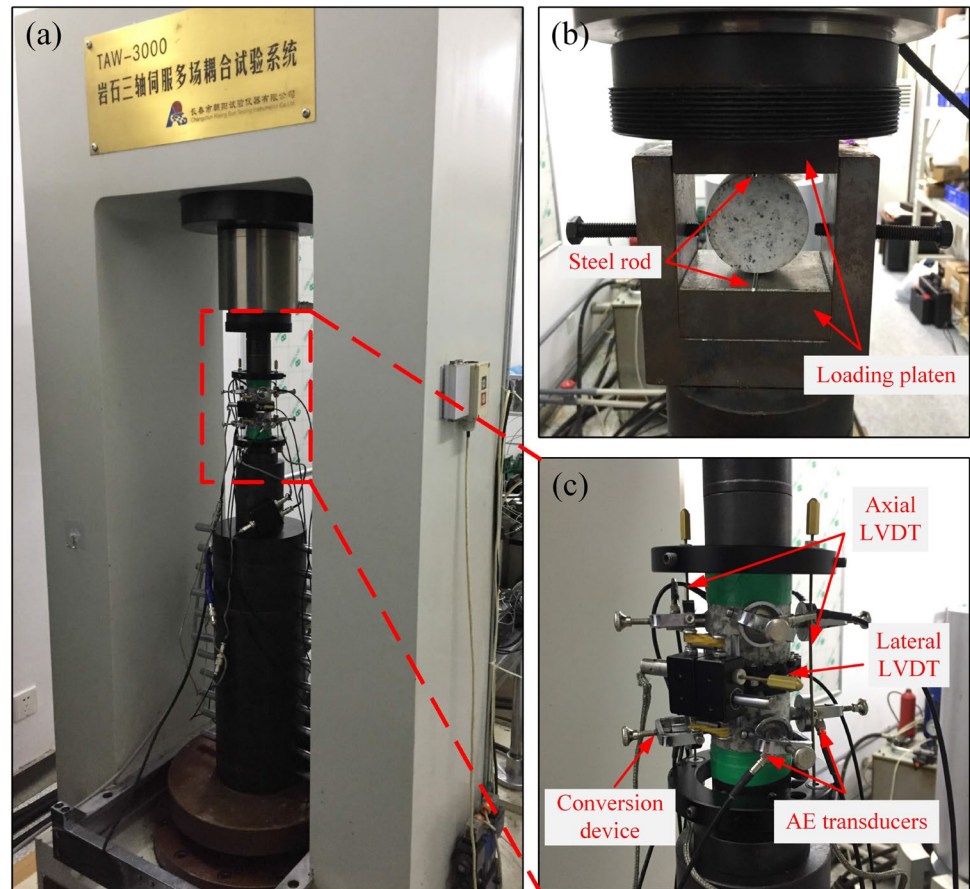


Fig. 3 Photographs of **a** TAW-3000 hydraulic servo-controlled compression system; **b** Brazilian splitting test loading configuration; and **c** cylindrical specimen assembled with two LVDT and eight AE transducers



convenience in preparing samples and conducting tests (Peras and Diederichs 2014; Sha et al. 2019). Figure 3b shows the loading configuration used in the Brazilian splitting test, which consists of two loading platens and two small-diameter steel rods. This configuration enables the line load to pass through the tested sample along the diameter. Throughout the test, a constant loading rate of 200 N/s was applied on the disk sample until failure according to the suggestions of ISRM (Ulusay and Hudson 2007). The axial load and axial displacement were automatically recorded by the load control software. Three disk samples were tested under each cycle condition. The Brazilian tensile strength (BTS) can be calculated by the following equation:

$$\sigma_t = \frac{2P}{\pi dt}, \quad (3)$$

where σ_t is BTS of the sample, P is the load at failure, d is the diameter of the sample, and t is the thickness of the sample.

The unconfined compression tests were conducted to determine the uniaxial compressive strength (UCS) and deformation behavior of the granite samples subjected to different heating–cooling cycles, and three cylindrical

samples were tested for each treatment condition. As shown in Fig. 3c, the axial and lateral linear variable differential transformers (LVDT) were used to measure the deformation in the corresponding direction during compression. The measurement ranges of axial and lateral LVDTs are 2.5 and 6.5 mm, respectively, and both have an accuracy of 0.01%. Before conducting the compression tests, the two LVDTs were carefully calibrated to ensure the veracity of deformation data. Under the load controlled by axial deformation, the rock sample was compressed at a rate of 0.02 mm/min until failure.

In addition, AE technology was also employed in this study to monitor the microcrack activity of rocks during compression in real time. As pointed out by Mansurov (1994), AE is a phenomenon in which the strain energy is suddenly released in the form of transient elastic waves since the structure of a material changes under external force. It can reflect the initial damage and the progressive failure processes of rocks, thereby is widely used in the field of rock mechanics (Hardy 1994; Kim et al. 2015). In the present study, the AE parameters of the granite sample during compression test were recorded by a DS2 series full information AE signal analyzer. For purpose of covering the volume of the rock sample as completely as possible, eight

AE piezo ceramic transducer were symmetrically mounted approximately 25 mm away from both ends of the sample by means of the conversion devices (see Fig. 3c). Moreover, the interfaces between the AE transducers and the conversion devices were coated with Vaseline film to achieve a good acoustic coupling (Zhang et al. 2015; Zhao et al. 2013). The coupling effect between them was checked through the pencil lead fracture tests, in which the amplitude of the AE signals caused by the pencil leads fracturing should be not less than 95 dB. To reduce the effect of environment noise and ensure the reliability of AE signals, the gain value of the pre-amplifier and the threshold for AE detection were set to 40 dB and 50 dB, respectively (Rong et al. 2018).

3 Experimental Results and Analysis

3.1 Changes in Physical Properties

3.1.1 Mass, Volume and Density

Figure 4 shows the changes in M , V and ρ of granite samples after different heating–cooling treatments. It can be seen that as the number of cycles increases, the decline magnitude of M gradually increases, while the reduction rate shows a downward trend (see Fig. 4a). Actually, the dehydration of minerals is one of the primary factors leading to the reduction in M of the sample. Previous researches have shown that minerals in the rock generally undergo different dehydration reactions at different temperature intervals (Sun et al. 2015). For instance, the absorption water will escape from the surface of the mineral or the pores between minerals at around 100 °C, and the crystal water can get rid of the constraint of the mineral lattice before 400 °C (Zhang et al. 2016; Hu et al. 2018). The repeated heating treatments gradually enhance the dehydration effect of minerals, thereby resulting in a continuous reduction in M of the granite sample. In addition, fine surface grains on the sample may flake in the process of cyclic heating–cooling, which is also the reason for the decrease of M .

As shown in Fig. 4b, V of the sample gradually increases with increasing heating–cooling cycles, but the increment rate of V exhibits a reducing trend. The generation of thermal stresses during heating will cause the initiation and growth of micro-defects in the granite, which expand the void space of the rock. Such microstructural damage is continuously accumulated as the number of cycles increase, thus leading to a gradual expansion in volume of the granite samples. On the other hand, the increase in pore space will in turn affect the level of thermal stress and slow down the volume expansion of the rock. The relevant mechanism is stated in detail in

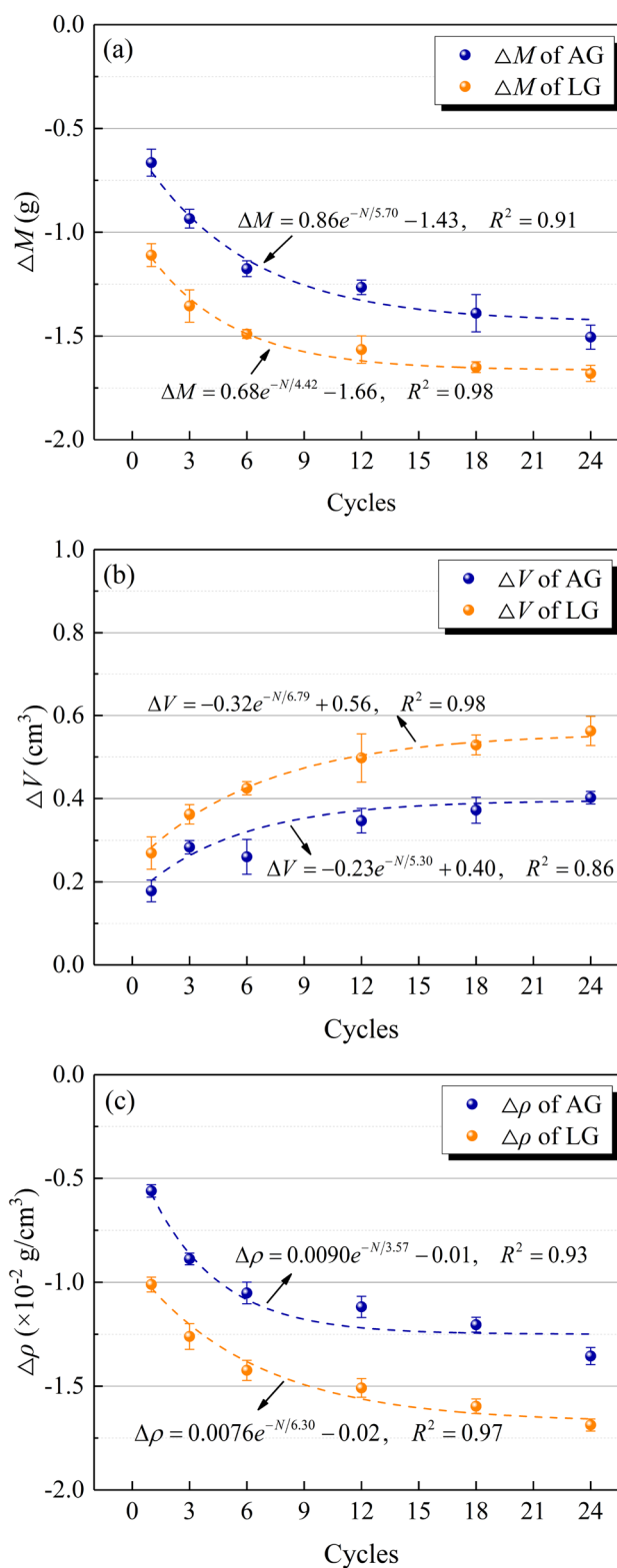


Fig. 4 Changes in **a** mass **b** volume and **c** density of granite samples after different heating–cooling cycles

Sect. 4.1. Due to the decrease of M and the increase of V , ρ of the sample naturally presents a decreasing trend as the number of cycles increase (see Fig. 4c).

It is found from Fig. 4 that LN₂ cooling has a more significant impact on the above physical properties of high-temperature granite. The change magnitudes of M , V and ρ of the LG sample are dramatically greater than that of the AG sample at each cycle condition. When the high-temperature sample are subjected to LN₂ quenching, the intense thermal shock will be induced in the rock because of the rapid thermal exchange between cryogenic LN₂ and high-temperature granite (Cai et al. 2014a; Han et al. 2018). This leads to a more severe deterioration of these physical properties of the LG sample. In addition, it is found that there is a distinct appearance damage of the LG sample after exposure to LN₂ cooling. Taking the samples subjected to 12–24 heating–cooling cycles as the examples, the appearance characteristics of these samples were carefully inspected by a high-definition camera, as shown in Fig. 5. It is seen that the visible macro-defects appear on the surface of the LG sample after 12 cyclic treatments (see Fig. 5a–c), whereas not observed on the surface of the AG sample under the same cycle number (see Fig. 5d–f). This can well explain why the reduction in M of the LG sample is obviously larger than that of the AG sample.

3.1.2 Porosity and P-Wave Velocity

Porosity and P-wave velocity are two important physical properties of rock materials and are widely used to characterize the structural integrity of the rock (Reuschlé et al. 2006). Figure 6 presents the magnitude and corresponding change rate of P and V_p of the granite samples after different heating–cooling cycles. The detailed measurement values of the two parameters are listed in Table 3.

As shown in Fig. 6, for the intact granite sample (i.e., no heating–cooling treatments), the average values of P and V_p are about 0.82% and 4430 m/s, with the standard deviation of 0.01 and 26, respectively. This implies that the granite samples tested in this study are intact in nature state and similar in pore development. Generally, no matter what cooling method is adopted, P of the granite gradually increases as the increase in cycles (see Fig. 6a), while the variation in V_p with cycles is reverse (see Fig. 6b). From 0 to 12th cycles, the average P values increase by 32.93% and 57.32%, and the average V_p values decrease by 35.20% and 42.56% for the AG and LG samples, respectively. After that, the P and V_p of the granite samples nearly almost constant irrespective of the cooling method. This indicates that the influence of heating–cooling treatments on internal structures of the rock become weaker after 12 cycles. In addition, it is found no matter the increase in P or decrease in V_p of the LG sample under each cyclic condition, when compared to that of the AG sample, are of larger magnitude (see Fig. 6).

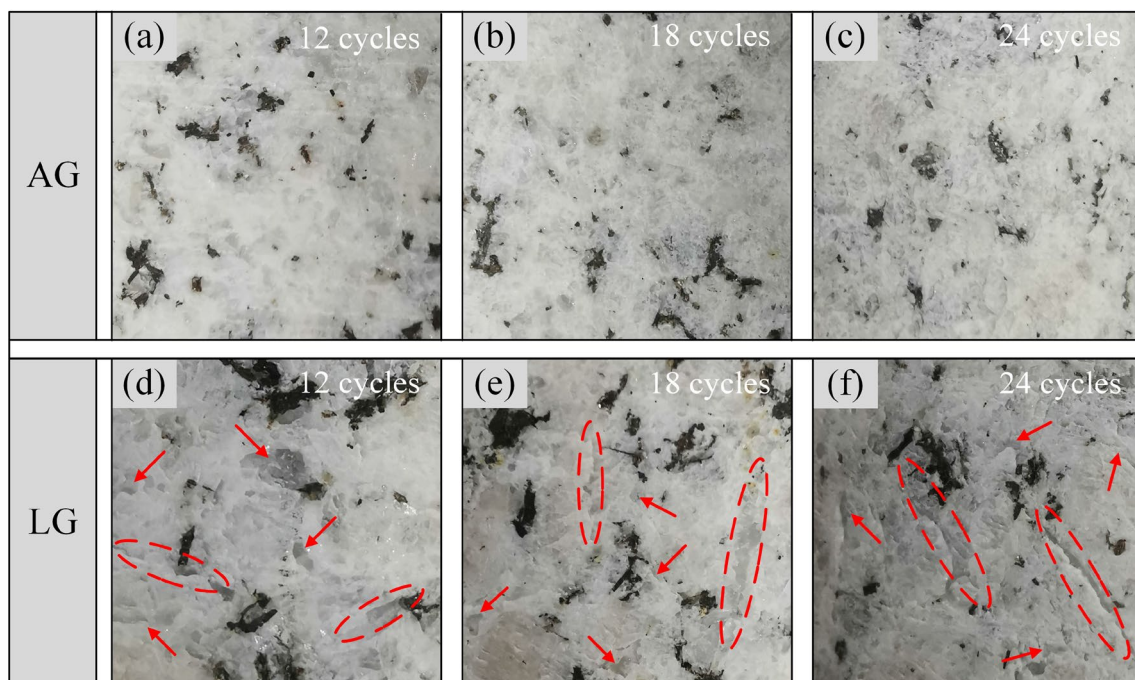


Fig. 5 Appearance photographs of granite samples after different heating–cooling cycles (arrows and ellipses indicate the location of flaking points)

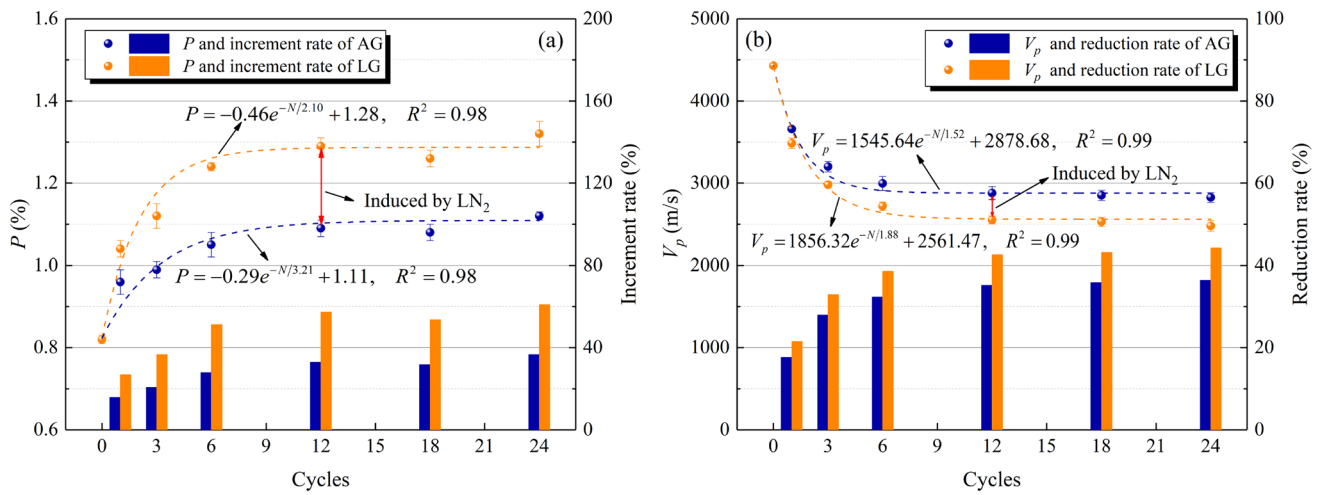


Fig. 6 Variations and change rate of **a** porosity and **b** P-wave velocity of granite samples after different heating–cooling cycles

Table 3 Summary of average values of physico-mechanical properties of granite samples after cyclic heating–cooling treatments

| Cycles | AG sample | | | | | | LG sample | | | | | |
|--------|--------------|----------------------------|-----------|-----------|----------------|----------------------------------|--------------|----------------------------|-----------|-----------|----------------|----------------------------------|
| | <i>n</i> (%) | <i>V_p</i> (m/s) | UCS (MPa) | BTS (MPa) | <i>E</i> (GPa) | ϵ_p (10 ⁻³) | <i>n</i> (%) | <i>V_p</i> (m/s) | UCS (MPa) | BTS (MPa) | <i>E</i> (GPa) | ϵ_p (10 ⁻³) |
| 0 | 0.82 | 4430 | 160.37 | 5.42 | 70.11 | 3.30 | 0.82 | 4430 | 160.37 | 5.42 | 70.11 | 3.30 |
| 1 | 0.96 | 3659 | 154.60 | 4.72 | 67.24 | 3.49 | 1.04 | 3486 | 146.88 | 4.31 | 63.46 | 3.68 |
| 3 | 0.99 | 3200 | 152.89 | 4.46 | 67.49 | 3.54 | 1.12 | 2980 | 138.63 | 3.94 | 57.01 | 3.97 |
| 6 | 1.05 | 2996 | 142.01 | 3.85 | 59.62 | 3.98 | 1.24 | 2719 | 135.52 | 3.04 | 53.66 | 4.08 |
| 12 | 1.09 | 2879 | 135.21 | 3.44 | 53.49 | 4.05 | 1.29 | 2552 | 123.62 | 2.38 | 48.67 | 4.23 |
| 18 | 1.08 | 2850 | 134.13 | 3.51 | 49.43 | 4.29 | 1.26 | 2528 | 124.41 | 2.25 | 44.93 | 4.27 |
| 24 | 1.12 | 2825 | 134.73 | 3.22 | 50.98 | 4.12 | 1.32 | 2478 | 120.61 | 2.52 | 43.90 | 4.42 |

Apparently, an increase in *P* or decrease in *V_p* is an indication of micro-defects growth in the rock. As explained earlier, high-temperature treatment causes the generation of thermal stresses between adjacent minerals. The grain boundary or intragranular microcracks are induced inside the granite sample once the thermal stress destroys the cementation between minerals (see Sect. 3.4), which subsequently leads to a change in *P* and *V_p* of rocks. The repeated cyclic treatments provide the required energy for the propagation of the microcracks. Therefore, a more significant microstructural damage is found in the sample after more heating–cooling cycles. Moreover, compared with air cooling, the rapid cooling treatment with cryogenic LN₂ induces additional thermal shock microcracks, thus aggravating the damage to the pore structure of the rock sample.

3.2 Changes in Mechanical Properties

3.2.1 Stress–Strain Curve

The stress–strain curve provides a fundamental understanding for the mechanical behavior of rocks during compressive

loading. It is generally accepted that the axial stress–axial strain curve of the rock under unconfined condition can be divided into five stages (see Fig. 7), i.e., (1) crack closure, (2) elastic deformation, (3) stable crack growth, (4) unstable crack growth, and (5) post-peak deformation stages (Martin and Chandler 1994; Brace et al. 1966; Cai et al. 2004; Peng et al. 2015; Rong et al. 2018).

The representative axial stress–strain curves of the granite samples after different cyclic heating–cooling are illustrated in Fig. 8. As shown in Fig. 8a, c, the axial stress–axial strain curves of the samples exhibit a concave upward shape during initial loading. Many studies have pointed out that this nonlinear deformation of the rock is associated with the closure of pre-existing microcracks inside rocks during loading (Bieniawski 1967; Yang et al. 2017a). In general, the nonlinear behavior of the rock at this stage becomes more prominent as the number of cycles increases, especially for the sample cooled by cryogenic LN₂. In addition, it is seen from Fig. 8b, d that the sample subjected to more heating–cooling cycles usually has more distinct volumetric compression. These phenomena indicate that more thermal cracks are induced in the rock due to the increased heating treatments

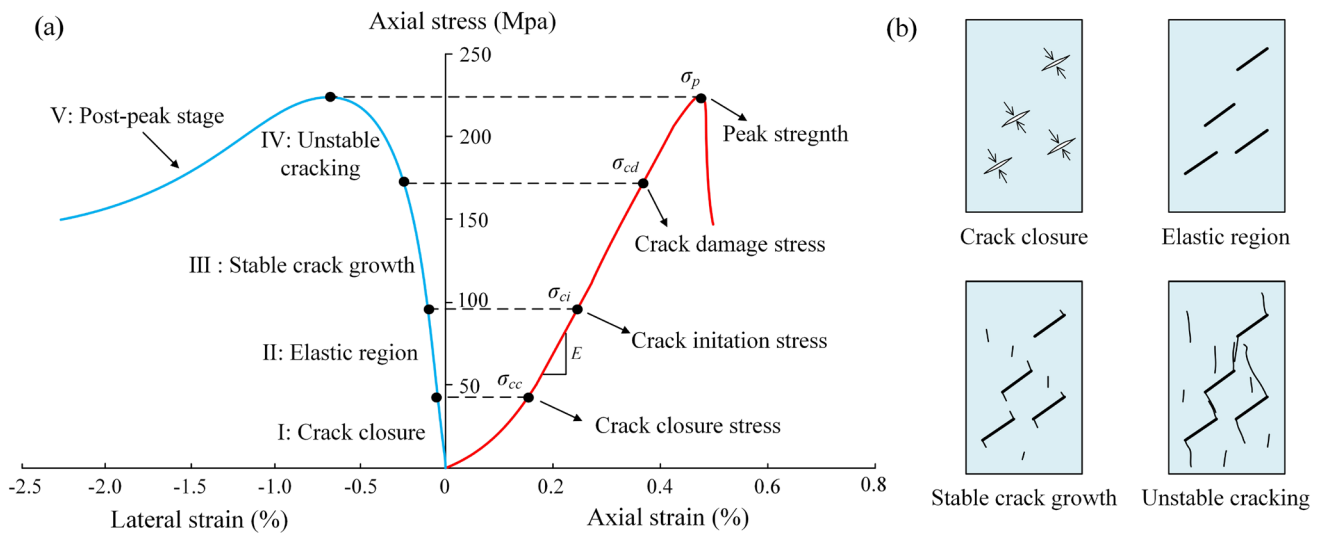


Fig. 7 A stress–strain diagram of rock in uniaxial compression test (modified from Martin and Chandler 1994 and Peng et al. 2015). **a** Various deformation and stress thresholds are identified from the stress–strain curves; **b** a schematic representation showing different crack behaviors

and cooling rate. After the stage of crack closure, the granite sample shows a linear elastic deformation, that is, the axial stress increases approximately linearly with the axial strain. It is generally believed that no new microcracks are generated at this stage. The Young’s modulus (E) of the rock can be determined based on the linear variation of the curve. As the further increase of axial load, the axial stress–axial strain curve gradually deviates from the linear behavior due to the initiation, extension and coalescence of microcracks. Thereafter, the sample reach the peak strength and enter the post-peak deformation stage. As seen from Fig. 8, the influence of the number of cycles or cooling rate on the post-peak deformation of the sample seem to be not remarkable. A sudden stress drop following the peak stress can be found at this stage for almost all granite samples, implying that they all failed in a form of brittle failure (Siratovich et al. 2016).

3.2.2 Strength Characteristic of Rock

Changes in UCS and BTS of the granite sample with the number of heating–cooling cycles are plotted in Fig. 9. The average values of UCS and BTS of the rock for each cycle are listed in Table 3. It is found that the mechanical properties of the sample greatly depend on the number of cycles and cooling methods. From Fig. 9, both the compressive and tensile strength of the sample gradually decline as the number of cycles increase. However, the decrease magnitudes in these two mechanical parameters of the LG sample at each heating–cooling cycle are more remarkable than that of the AG sample. For instance, the average UCS of LG sample is reduced by 24.8% after 24 cyclic treatments, whereas only 16.0% for AG sample (Fig. 9a). In like manner, the

attenuation rate of BTS for the LG and AG samples subjected to 24 heating–cooling cycles are 53.5% and 40.6%, respectively (Fig. 9b). Such cases can be attributed to the fact that far more severe damage are caused in the rock during LN₂ rapid cooling. In contrast, the attenuation amplitude of BTS of the sample is more remarkable than that of UCS. The results of Kim et al. (2013) and Shao et al. (2014) indicate that the transient thermal stress caused by rapid cooling is normally tensile at the surface of the rock. Generally, the granite has the lower resistance to the tensile stress than any other kind of stress, making it more prone to failure under tensile conditions. In addition, it is also found from Fig. 9 that the reduction in UCS and BTS of the sample mainly occurs within the initial 12 cycles, which is consistent with the variations of porosity and P-wave velocity described in Sect. 3.1.2.

As presented in Fig. 7a, several stress thresholds, which are termed as the crack closure stress σ_{cc} , the crack initiation stress σ_{ci} , the crack damage stress σ_{cd} and the peak strength σ_p (i.e., UCS), can be identified from the progressive failure process of rocks during axial loading (Martin and Chandler 1994; Cai et al. 2004). Although various methods have been proposed by researchers based on stress–strain curve or AE parameter to determine the stress thresholds, they are different in terms of applicability, conveniences and subjectivity. In the present study, the σ_{cc} , σ_{ci} and σ_{cd} of the rock sample were determined using axial strain response (ASR) method (Peng et al. 2015), lateral strain response (LSR) method (Nicksiar and Martin 2012) and volumetric strain method (Brace et al. 1966; Bieniawski 1967), respectively.

The stress thresholds and their ratios to σ_p for the granite samples subjected to different heating–cooling treatments

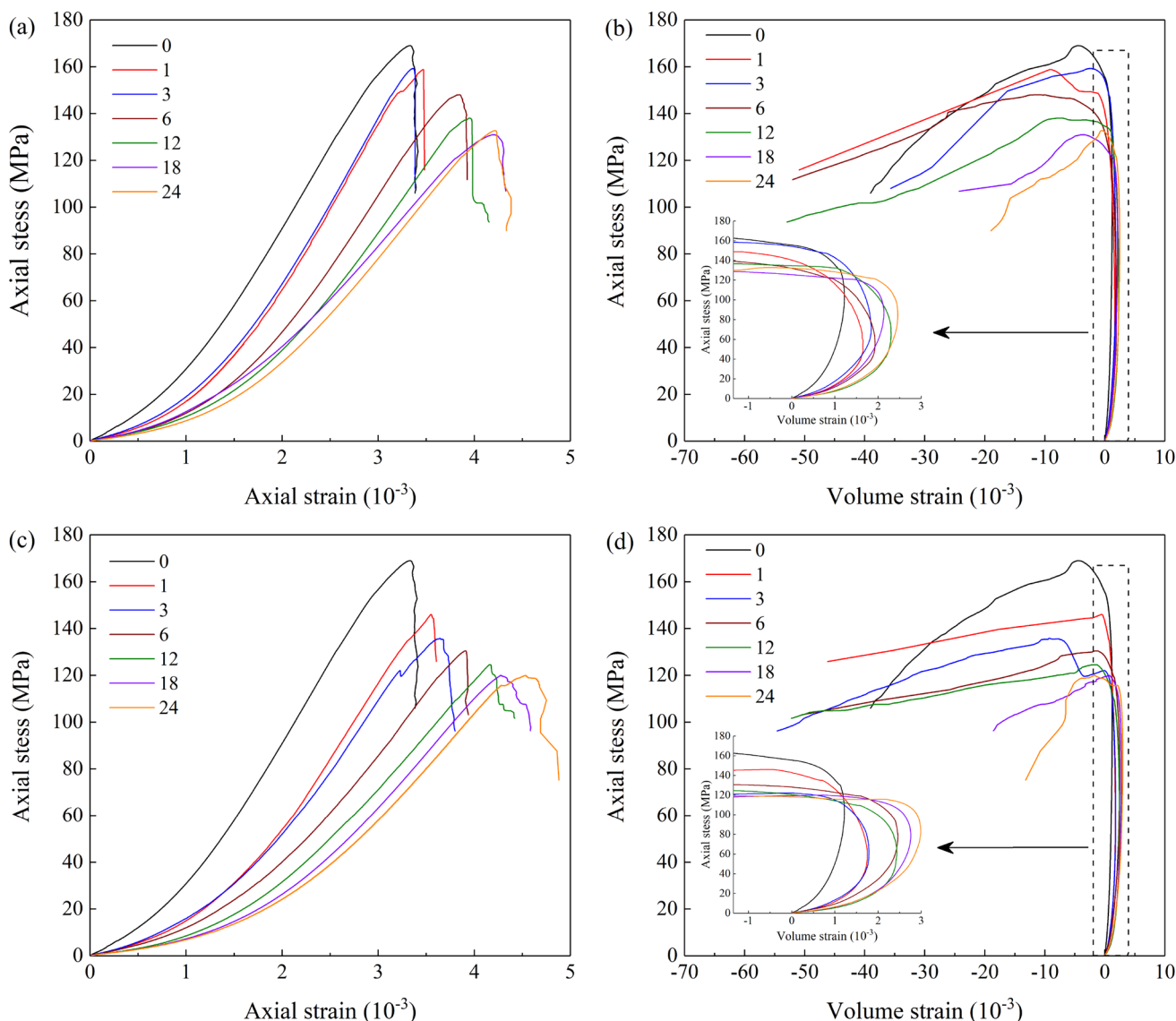


Fig. 8 Stress–strain curves of granite samples after different heating–cooling cycles. **a, b** Air cooling, and **c, d** LN₂ cooling

are summarized in Table 4. It is seen that σ_{cc} , σ_{ci} and σ_{cd} of the sample without thermal damage (i.e., 0 cycle) were 32.8, 55.15 and 111.02 MPa, respectively. Figure 10 presents the changes of the stress thresholds with the number of heating–cooling cycles. As the figure shows, the magnitude of σ_{ci} and σ_{cd} generally show a trend of decrease with the increasing cycles, regardless of the cooling method. The variation in σ_{cd} is found to be more sensitive to the number of the cycles than σ_{ci} . However, there is only slight fluctuation for σ_{cc} as the number of cycles increases. In addition, it is seen from Fig. 10 that σ_{cc} and σ_{ci} show similar change amplitude with cycles for the AG and LG samples, while σ_{cd} observed under the LN₂ cooling condition is distinctly lower.

The ratios of stress thresholds to σ_p of the granite samples after exposure to different heating–cooling cycles are

illustrated in Fig. 11. It is seen that no matter which cooling method is adopted, the value of σ_{cc}/σ_p gradually increase with the increase in the number of cycles, but is opposite for the values of σ_{ci}/σ_p and σ_{cd}/σ_p . Correspondingly, the crack damage presents different variation tendencies with the increase in cycle number, that is, increase of the crack closure region and the unstable crack propagation region, decreases of the elastic deformation region and the stable crack propagation region. The results are basically consistent with those of Kumari et al. (2017). The increase in crack closure region indicates that more severe initial damage has occurred in the rock sample undergone more cyclic treatments. The progressive decrease of the elastic deformation region is probably related to that the brittle characteristic of the rock sample is weakened as the number of cycles

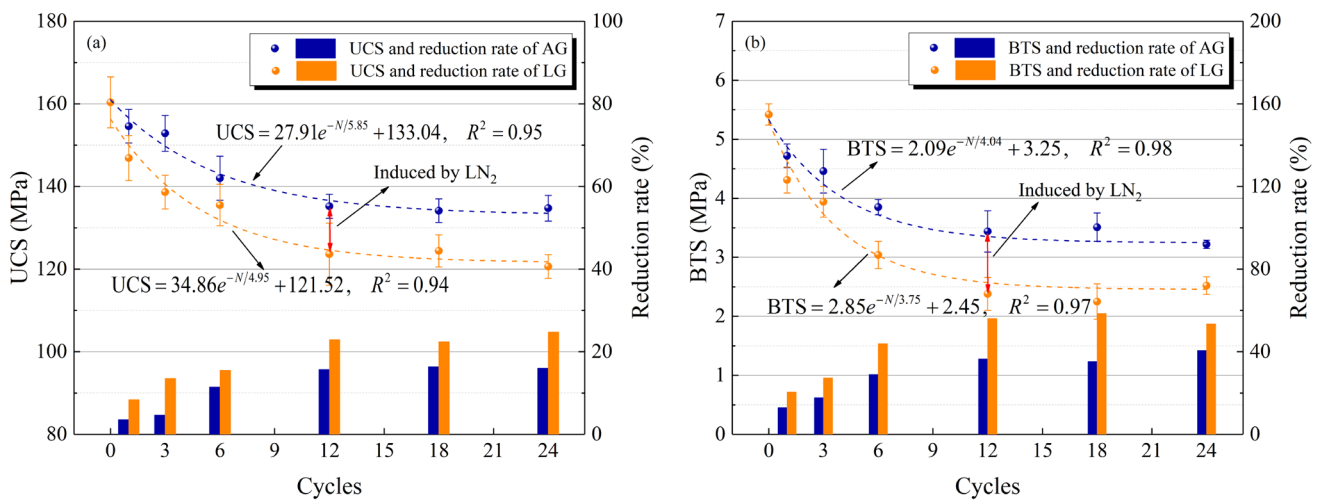


Fig. 9 Variations and change rate of a compressive strength and b tensile strength of granite samples after different heating-cooling cycles

increases. In contrast, the amplitude of the decrease of stable crack propagation region and the increase of unstable crack propagation region for the LG sample are more remarkable than the AG sample, especially after more cycles. This implies that increasing number of cycles and cooling rate will accelerate the development of microcracks during loading.

3.2.3 Deformation Characteristic of Rock

Figure 12a shows the changes of E of the granite sample with respect to the number of cycles, and the detailed test data are presented in Table 3. As with the mechanical strength, the number of cycle and cooling method have significant influence on E of the rock. As shown in Fig. 12a, E presents a decreasing trend as the number of cycles increase. After 24 heating-cooling cycles, the E values of the AG and LG samples are 50.98 and 43.90 GPa, respectively, which attenuates by 27.29% and 37.38% compared to that of intact granite sample. In the same way, the decline magnitude of E gradually becomes smaller with the increasing cycles. When the heating-cooling treatment exceeds 12 cycles, the reduction rate of E is not remarkable. In addition, it is seen that E of the LG sample is distinctly lower than that of the AG sample at all cyclic conditions.

The failure strain (ϵ_p) is defined as the axial strain that corresponds the peak strength, which can reflect the deformation behavior of rock to some extents. The variation in ϵ_p with increasing heating-cooling cycles is shown in Fig. 12b. The results reveal that ϵ_p of the sample varies greatly due to the difference in cycle number and cooling method. From Fig. 12b, the value of ϵ_p gradually increases as the increase in the number of cycles, which is particularly prominent in the first several cycles. After 24 heating-cooling cycles, the

average ϵ_p of the AG sample has risen to 4.12×10^{-3} , which is 1.25 times of that for the intact sample. Compared with the AG sample, the LG sample usually has a larger ϵ_p for each cycle condition. The variations in ϵ_p indicates that the increase in the number of cycles and cooling rate leads to a greater ductility of the granite.

3.3 AE Characteristics

AE count rate and accumulative AE hit are two typical AE time-series parameters. They are selected to characterize the progressive failure process and microcrack behavior of the granite sample during loading in the current study. When an AE activity occurs, the oscillation number of a pulse signal crossing the threshold in unit time is termed as AE count rate (Peng et al. 2018). It is generally considered to be an effective indicator reflecting the intensity of the AE activity. The accumulative AE hit is defined as the accumulated value of the signal received by a transducer exceeding the threshold, which is on behalf of the number of AE activities (Eberhardt et al. 1998).

The variations in axial stress, AE count rate and accumulative AE hits with axial strain of the intact granite sample are illustrated in Fig. 13. It is evident that there is a good correlation between the evolution in the AE parameters and the stress-strain curve. Generally, the AE activity occurs in the initial deformation stage is related to the closure of the pre-existing microcracks inside the rock (Yang et al. 2017a). As shown in Fig. 13, almost no AE activity is monitored at the initial loading stage for the granite sample without treatment, indicating that only very few micro-defects exist inside the natural granite sample. Afterwards, the number of AE hit presents an obvious increasing trend with the axial load increases, while the AE count rate still remain a low

Table 4 Stress thresholds and normalized ratios of granite samples after different heating–cooling cycles

| Cycles | AG sample | | | | | | LG sample | | | | | |
|--------|---------------------|---------------------|---------------------|---------------------|-------------------------------|-------------------------------|---------------------|---------------------|---------------------|---------------------|-------------------------------|-------------------------------|
| | σ_{cc} (MPa) | σ_{ci} (MPa) | σ_{cd} (MPa) | σ_{cp} (MPa) | σ_{cc}/σ_{cp} (%) | σ_{cd}/σ_{cp} (%) | σ_{cc} (MPa) | σ_{ci} (MPa) | σ_{cd} (MPa) | σ_{cp} (MPa) | σ_{cc}/σ_{cp} (%) | σ_{cd}/σ_{cp} (%) |
| 0 | 32.80 | 55.15 | 111.02 | 160.37 | 20.74 | 70.24 | 32.80 | 55.15 | 111.02 | 160.37 | 20.74 | 70.24 |
| 1 | 25.67 | 46.39 | 97.45 | 154.60 | 16.61 | 67.08 | 25.36 | 48.35 | 99.02 | 146.88 | 17.27 | 36.88 |
| 3 | 26.39 | 51.83 | 102.38 | 152.89 | 16.93 | 65.71 | 22.29 | 44.56 | 91.40 | 138.63 | 16.08 | 37.16 |
| 6 | 23.51 | 47.10 | 94.61 | 142.01 | 16.23 | 66.28 | 22.55 | 45.79 | 86.59 | 135.52 | 16.66 | 36.83 |
| 12 | 23.17 | 49.27 | 87.53 | 135.21 | 17.15 | 64.75 | 20.67 | 45.22 | 80.67 | 123.62 | 17.52 | 34.50 |
| 18 | 25.70 | 45.03 | 86.99 | 134.13 | 19.17 | 64.86 | 21.63 | 44.18 | 78.53 | 124.41 | 18.98 | 35.51 |
| 24 | 20.70 | 41.16 | 82.11 | 134.73 | 18.97 | 61.95 | 20.97 | 38.32 | 74.23 | 120.61 | 19.90 | 30.80 |

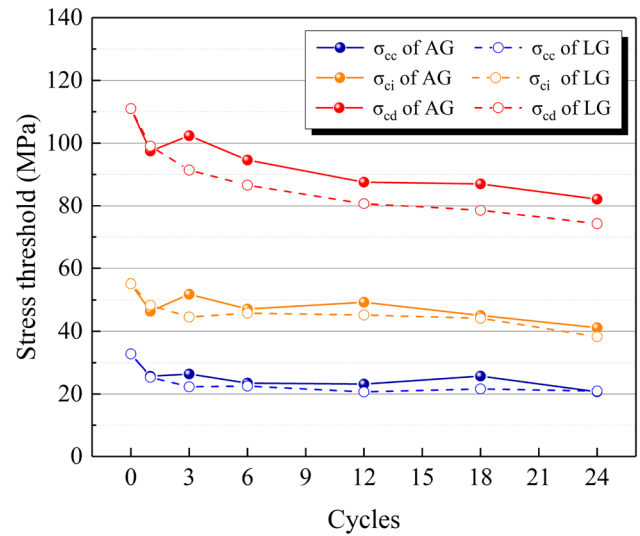


Fig. 10 Changes of stress thresholds of granite samples after different heating–cooling cycles

level. This implies that a great number of tiny fractures are generated in the rock during this process. With the further increases of axial stress, the AE count rate with a larger magnitude begin to appear intensively, and is strongest near the peak strength. But at the same time, the increment rate of accumulative AE hits becomes slower. These phenomena indicate that the cracks induced in the rock are larger in scale than before, but relatively less in number. In addition, it is also seen that the “sudden stress drop” on the stress–strain curve corresponds to a sharp increase in the AE count rate. It can be attributed to the fact that the transient stress relaxation induced by dislocation or breakage of minerals or grain boundary movement in the rock during loading (Peng and Yang 2018).

Figures 14, 15 show the evolution in AE parameters of AG and LG samples during uniaxial compression for different cyclic heating–cooling conditions, respectively. In general, the overall variation trends of AE count rate and accumulative AE hits of the granite samples after different cyclic treatments are basically similar with that of the intact sample, except during the initial loading stage. Compared with the intact granite sample, both the AE count rate and accumulative AE hits of the AG and LG samples are stronger at the initial loading stage, and gradually enhanced as the number of cycles increases (see Figs. 14 and 15). It can be concluded that the number of thermal cracks in the rock greatly increases when more heating–cooling treatment is applied, that is, more severe initial damage is induced in the rock. At the same number of heating–cooling cycles, the AE count rate of LG samples at initial deformation stage is generally denser and higher than that of the AG samples. This further

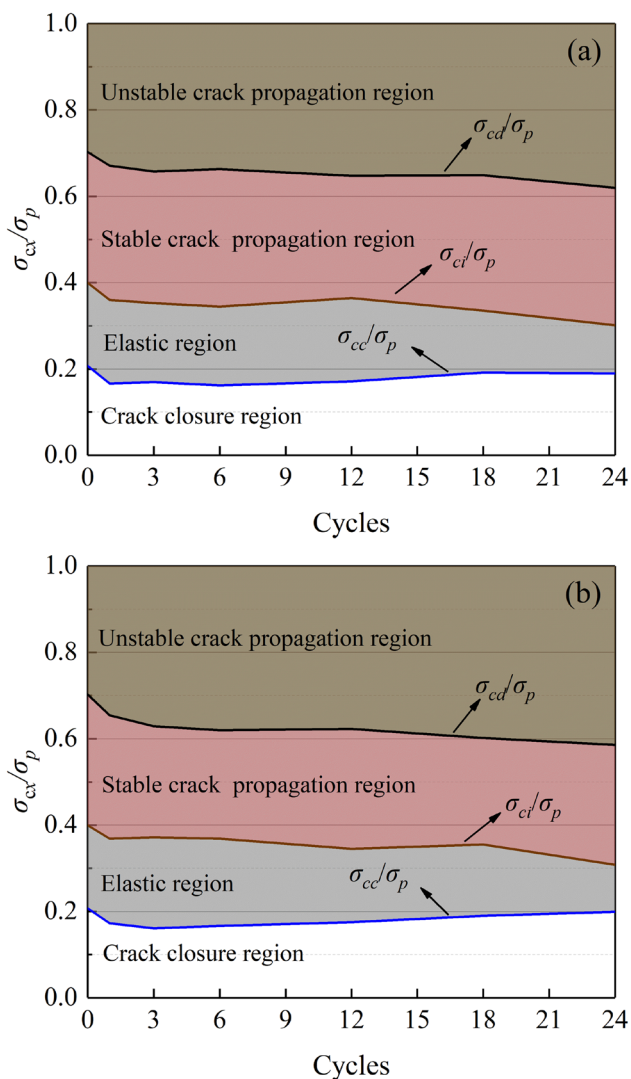


Fig. 11 Stress threshold ratios of **a** air cooled samples and **b** LN₂-cooled samples after different heating-cooling cycles

demonstrates that the rapid LN₂ quenching can exacerbate the microstructural damage to the high-temperature rocks.

The final number of AE hits of the granite samples versus different heating-cooling conditions is plotted in Fig. 16. It is seen that, with the increase in the number of cycles, the accumulative AE hits of AG and LG samples generally show an increasing trend, which is mainly associated with the initial microcracks induced by thermal shock inside the rock sample. Furthermore, for each heating-cooling cycle, the final number of accumulative AE hits of LG sample after failure is greatly far higher than that of AG samples. This indicates that more microscopic fractures occur in the sample experienced LN₂ cooling treatment during loading.

3.4 Microstructural Alterations

In the current study, the microstructure of the granite samples after exposure to different heating-cooling cycles was observed with the aid of an Olympus BX53M polarizing microscope. Under each pretreatment condition, the thin slice with a side length of 2.5 mm and a thickness of about 0.03 mm was prepared. The microstructure of the rock sample was uniformly magnified by 50 times for the purpose of effectively identifying the development of grain boundary microcracks and intragranular microcracks.

Figures 17, 18 show the microphotographs of AG and LG samples after different heating-cooling cycles. As seen from Figs. 17a and 18a, the internal structure of the granite sample after 1 cycle has undergone some visible changes compared with that of the intact sample (see Fig. 1a). Although most of mineral grains in the granite sample are well cemented with each other, several grain boundary microcracks around quartz grains are identified. Under high-temperature condition, the uncoordinated thermal expansion behaviors between mineral grains lead to the generation of thermal stresses within the rock matrix. Once the maximum thermal stress exceeds the cementation strength of mineral grains, the new thermal cracks are induced. In addition, the anisotropic expansion of mineral grains along various crystallographic axes can also result in the microstructural damage upon heating (Hall 1999; Sirdesa et al. 2017). Quartz is the major diagenetic mineral of the granite used in this study, which has a larger thermal expansion coefficient than other minerals (Simmons and Cooper 1978; Kranz 1983). Hence, the grain boundary microcrack is more likely occurs near quartz grain boundary, which is consists with the observations of Fredrich and Wong (1986).

After three cycles, the grain boundary microcrack in the granite begin to develop gradually (see Figs. 17b and 18b). It is worth mentioning that the intragranular microcrack is observed in the LG sample after three heating-cooling cycles (see Fig. 18b), but that is found in the AG sample until six cycles (see Fig. 17c). Compared with air cooling, the repeated LN₂ cooling treatments cause more severe thermal shock damage to the high-temperature granite sample and provide more energy for the growth of the intragranular microcracks. It is clear from Figs. 17 and 18 that the microcracks in both AG and LG samples become denser as the number of cycles further increases, and the intragranular microcracks are easier identified, especially in the range of 12–24 cycles.

In addition, it is found that the width of microcrack is significantly affected by the number of cycles and cooling rate. As shown in Figs. 17 and 18, the microcrack in the rock after exposure to more cyclic treatments distinctly becomes wider. In contrast, the LG sample generally has a larger width of microcrack than that of the AG sample under

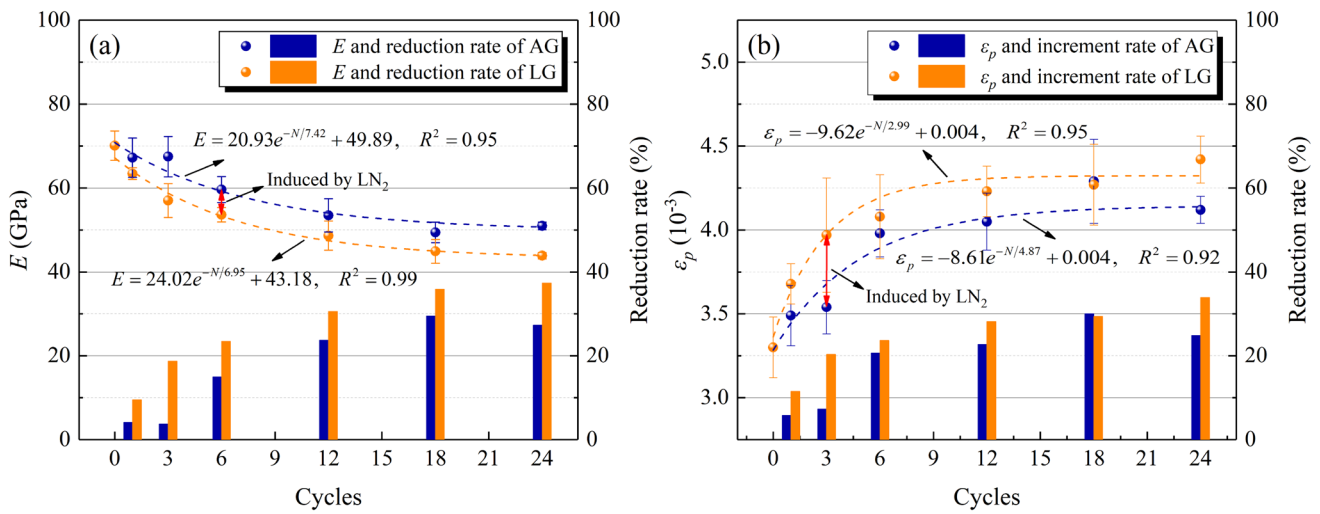


Fig. 12 Variations and change rate of **a** Young’s modulus and **b** failure strain of granite samples after different heating–cooling cycles

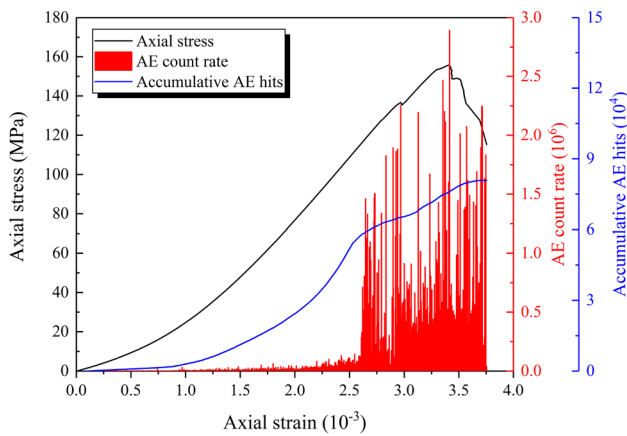


Fig. 13 Evolution of AE count rate and accumulative AE hits with axial strain for the intact granite sample

the same treatment condition. Taking 24 cyclic treatments as an example, the average width of microcrack in the AG sample measured by virtue of the image processing software is about 32 μm, while that in the LG sample achieve 48 μm.

4 Discussion

4.1 Analysis of Damage Evolution and Mechanism

According to the analysis in the previous sections, the cyclic heating–cooling treatment leads to distinct damage to the granite sample. In general, the exponential function is able to well describe the relationship between the physico-mechanical properties of rocks and the number of cycles. Taking advantages from these correlations, the damage variables

can be expressed as a function of UCS, BTS, E and V_p based on elastic strain theory. The damage variable can be calculated by Eq. (4) (Hueckel et al. 1994; Hu et al. 2018; Qin et al. 2020), and the calculated values of damage variables are given in Table 5.

$$D(I) = 1 - \frac{I_N}{I_0} \tag{4}$$

where I denotes the physical and mechanical parameters of rock (i.e., UCS, BTS, E and V_p), the subscript N denotes data obtained from the granite sample subjected to N heating–cooling cycles, and the subscript 0 denotes data obtained from the intact granite sample.

The relationship of different damage variables of AG and LG samples and the number of cycles is plotted in Fig. 19. As seen from the figure, regardless of the cooling method, the evolution of the four types of damage variable with the number of cycles basically follows an exponential law. The best fitting function of each damage variable is also given in Fig. 19, which all have a high correlation coefficient. In contrast, the damage extent of the AG and LG samples evaluated by BTS is the most significant, and followed by the damage evaluated by V_p , E and UCS (see Fig. 19). This is mainly related to the lower resistance of granite to tensile stress and the tensile failure generated during cooling. It is also clear from Fig. 19 that the damage variables increase rapidly in the first few cycles, while the growth rate of them gradually declines with the increasing cycles. In general, there is only a slight change in the damage variable after about 12 cycles, indicating that the internal damage of the rock sample almost reaches a stable state after that.

According to the microscopic observations in Sect. 3.4, the macroscopic damage of granite sample is the result of

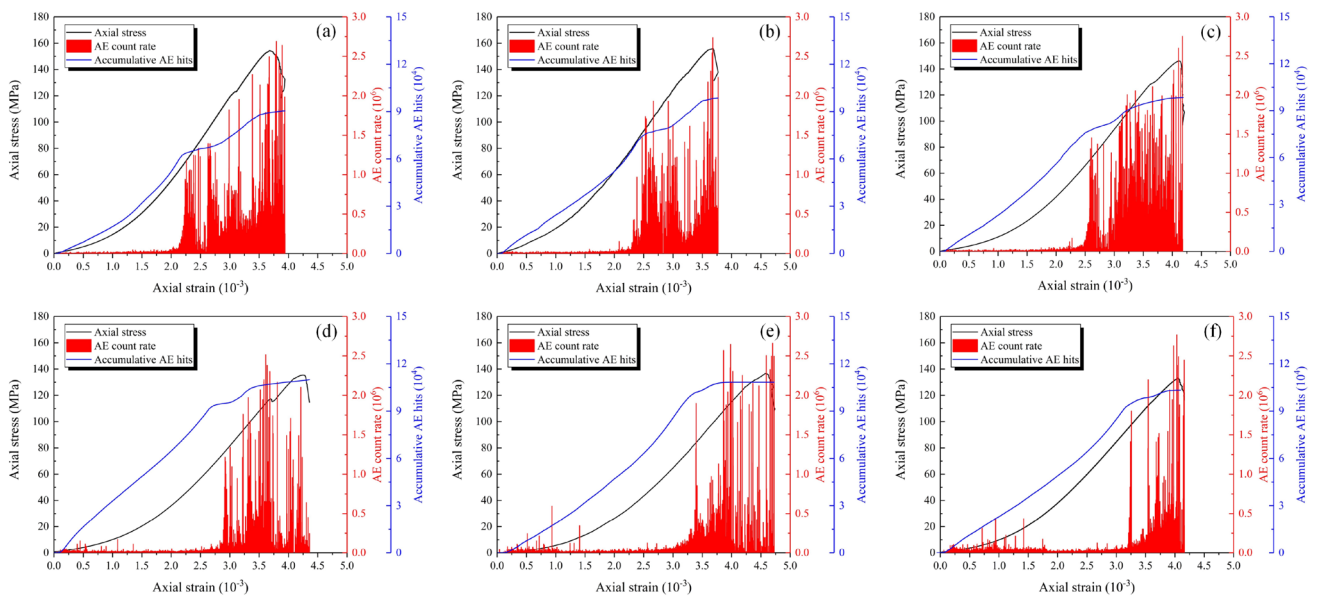


Fig. 14 Evolution of AE count rate and accumulative AE hits with axial strain for AG samples after different heating–cooling cycles. **a** 1 cycle, **b** 3 cycles, **c** 6 cycles, **d** 12 cycles, **e** 18 cycles, **f** 24 cycles

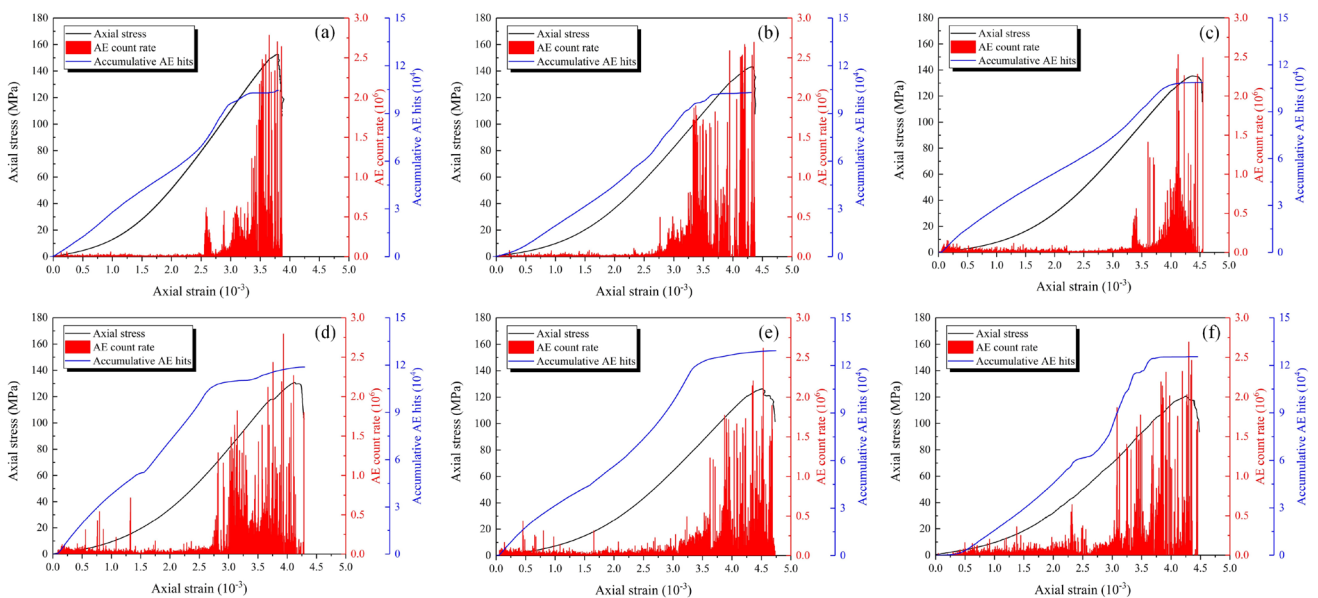


Fig. 15 Evolution of AE count rate and accumulative AE hits with axial strain for LG samples after different heating–cooling cycles. **a** 1 cycle, **b** 3 cycles, **c** 6 cycles, **d** 12 cycles, **e** 18 cycles, **f** 24 cycles

the initiation, propagation and coalescence of microcracks within the rock. In the first few heating–cooling cycles, the alternating thermal stress destroys the cementation between adjacent minerals and induces the growth of microcracks between or within the grains. This caused a distinct deterioration in the physico-mechanical properties of the rock. However, with a further increase in the number of heating–cooling cycles, the development of micro-defects provides sufficient deformation space for mineral expansion,

which reduce the level of thermal stress within the rock (Wu et al. 2019). Therefore, the degradation of the physico-mechanical behaviors of the granite is basically no longer aggravated after the threshold of cycles is reached.

In addition, it is seen that the damage extent of the LG sample is obviously larger than that of the AG sample. As listed in Table 5, the maximum values of the damage variables of the AG sample vary from about 0.164 and 0.406, while that of the LG sample is in the range of about

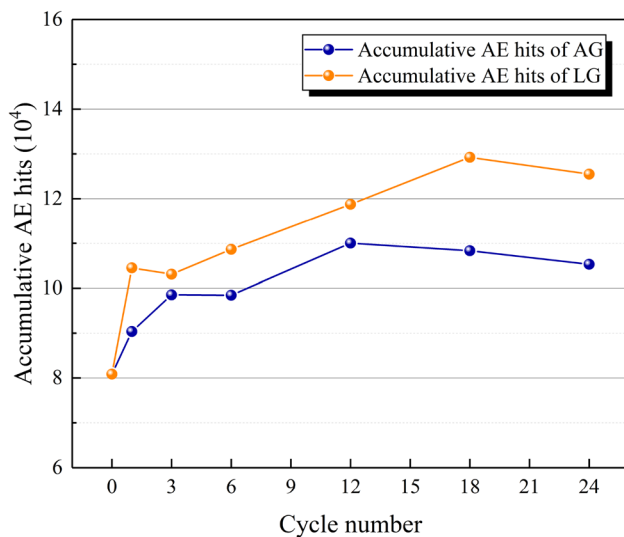


Fig. 16 Accumulative AE hits with of granite samples for different heating–cooling cycles

0.248–0.585. Different with the AG sample, the LG sample experienced an instantaneous, extreme temperature change during cooling. The temperature gradient during cooling process directly determines the magnitude of the thermal stresses generated in the rock (Wong and Brace, 1979). Unquestionably, the thermal stress induced by LN₂ cooling is far greater than that by air-cooling. Hence, a more

significant number of thermal cracks, that is, more severe damage, can be observed in the LG sample.

4.2 Correlation of P-Wave Velocity with Porosity and Strength Behavior

According to the above research results, it can be seen that the variation of V_p under different heating–cooling cycles correlates well with that of n and strength behavior of the rock. Since V_p is sensitive to the microstructure damage, it can indirectly reflect the change of pore structure of the rock. Meanwhile, the mechanical behaviors of rocks, including UCS and BTS, are significantly affected by the development of micro-defects. With that in mind, the correlation between n , UCS, BTS and V_p for the granite was investigated in this study. The relationships between them are shown in Fig. 20. As shown in the figure, n , UCS and BTS of the granite have a good linear relationship with V_p ($R^2 = 0.84, 0.80$ and 0.84). Compared with V_p , the determination of n , UCS and BTS is time-consuming, cumbersome, and expensive. Therefore, the porosity and mechanical strength of the rock can be quickly evaluated by the non-destructive V_p measurements.

4.3 Enlightenment of Current Work on Geothermal Exploitation

The experimental results in this study suggest that LN₂ has great potential in the field of geothermal reservoir

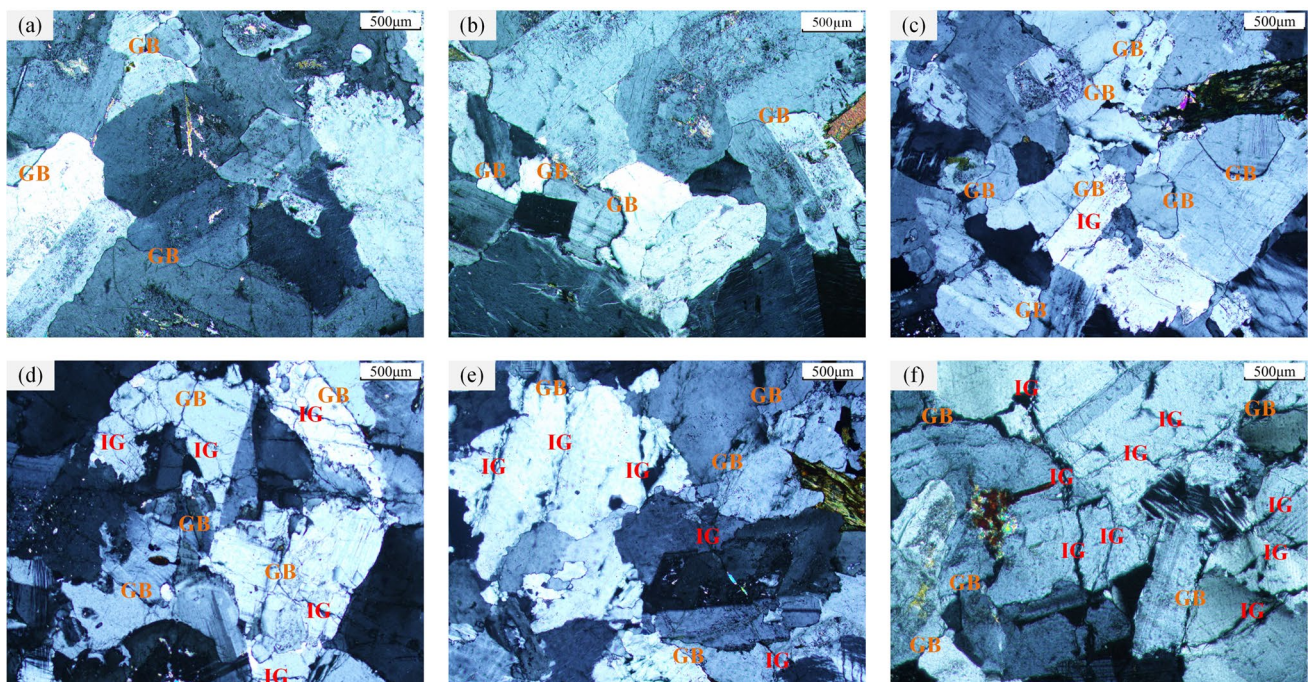


Fig. 17 Identification microcracks of AG samples after different heating–cooling cycles (GB–grain boundary microcrack, IG–Intragranular microcrack). **a** 1 cycle, **b** 3 cycles, **c** 6 cycles, **d** 12 cycles, **e** 18 cycles, **f** 24 cycles

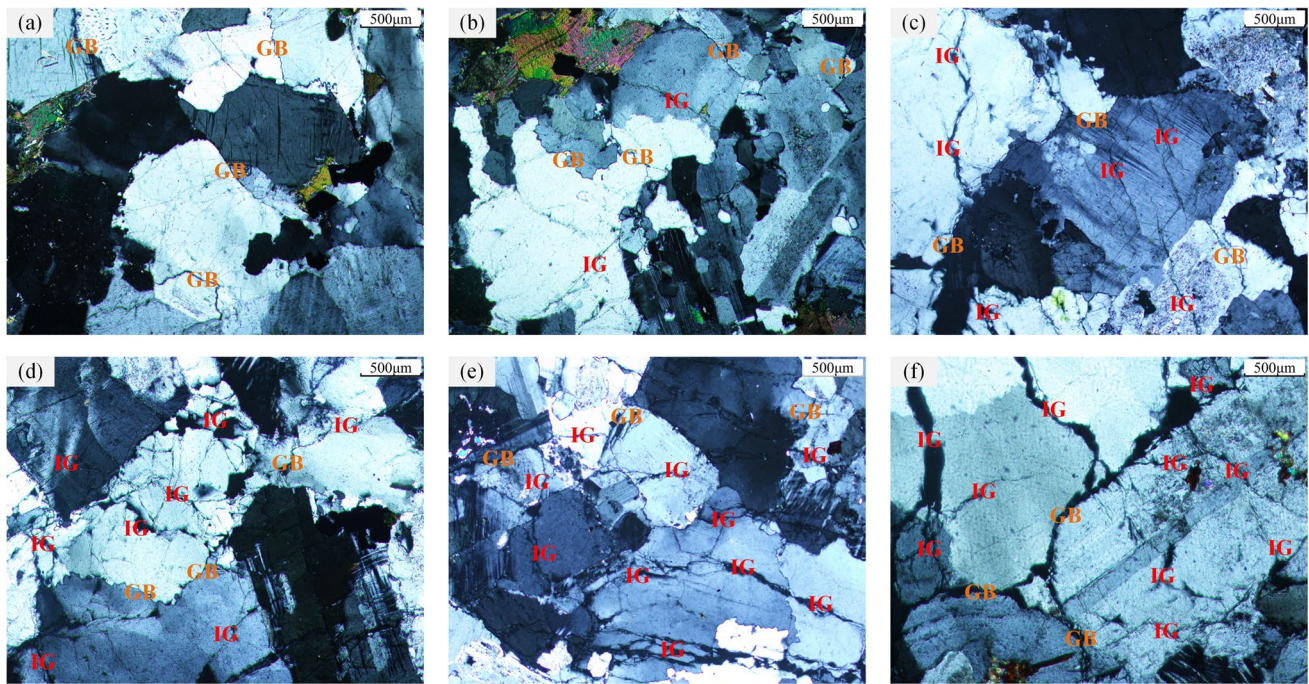


Fig. 18 Identification microcracks of LG samples after different heating–cooling cycles (GB–grain boundary microcrack, IG–Intragranular microcrack). **a** 1 cycle, **b** 3 cycles, **c** 6 cycles, **d** 12 cycles, **e** 18 cycles, **f** 24 cycles

Table 5 Damage variables of granite samples determined by different parameters

| Cycles | AG sample | | | | LG sample | | | |
|--------|-----------|----------|--------|----------|-----------|----------|--------|----------|
| | $D(UCS)$ | $D(BTS)$ | $D(E)$ | $D(V_p)$ | $D(UCS)$ | $D(BTS)$ | $D(E)$ | $D(V_p)$ |
| 0 | 0.000 | 0.000 | 0.000 | 0.000 | 0.000 | 0.000 | 0.000 | 0.000 |
| 1 | 0.036 | 0.129 | 0.041 | 0.174 | 0.084 | 0.205 | 0.095 | 0.213 |
| 3 | 0.047 | 0.177 | 0.037 | 0.278 | 0.136 | 0.273 | 0.187 | 0.327 |
| 6 | 0.115 | 0.290 | 0.150 | 0.324 | 0.155 | 0.439 | 0.235 | 0.386 |
| 12 | 0.157 | 0.365 | 0.237 | 0.350 | 0.229 | 0.561 | 0.306 | 0.424 |
| 18 | 0.164 | 0.352 | 0.295 | 0.357 | 0.224 | 0.585 | 0.359 | 0.429 |
| 24 | 0.160 | 0.406 | 0.273 | 0.362 | 0.248 | 0.535 | 0.374 | 0.441 |

stimulation. Actually, LN₂ fracturing utilizes the intense thermal shock induced by cryogen to break reservoir rocks, rather than merely relying on increasing fracturing pressure. With the injection of cryogenic LN₂ into HDR reservoir, the high-temperature rock experiences a rapid quenching process. The extreme thermal gradient results in considerable thermal shock damage to the rock and promote the generation and propagation of microcracks. Meanwhile, rapid cooling likely to cause tensile shrinkage cracking on the rock surface, which provides a passage for LN₂ to penetrate into the rock. The cyclic injection of LN₂ can not only further extends the pre-existing fracture channels, but also open up more new fractures inside the reservoir (Li et al. 2016; Elwegaa and Emadi 2018). In the meantime, a large number of secondary fractures are formed in the rock around the main fracture due to

the repeated thermal shock (Cai et al. 2016). Compared with the single LN₂ fracturing, the cyclic LN₂ fracturing is more likely to induce larger scale and more complex fracture networks (Wu et al. 2019). The formation of the desired complex fracture networks increases the contact area between the heat exchange medium and the HDR, which is great significant for improving the efficiency of geothermal energy exploitation. However, the current research work indicates that the damage of granite is not infinitely enhanced with the increase of LN₂ cooling cycles. After a certain number of cycles, the mechanical strength of the rock basically decayed to a stable value in this study. Therefore, when using LN₂ fracturing for reservoir stimulation, the permeability of the reservoir rock cannot be improved by blindly increasing the number of LN₂ injections. The optimal number of cyclic LN₂

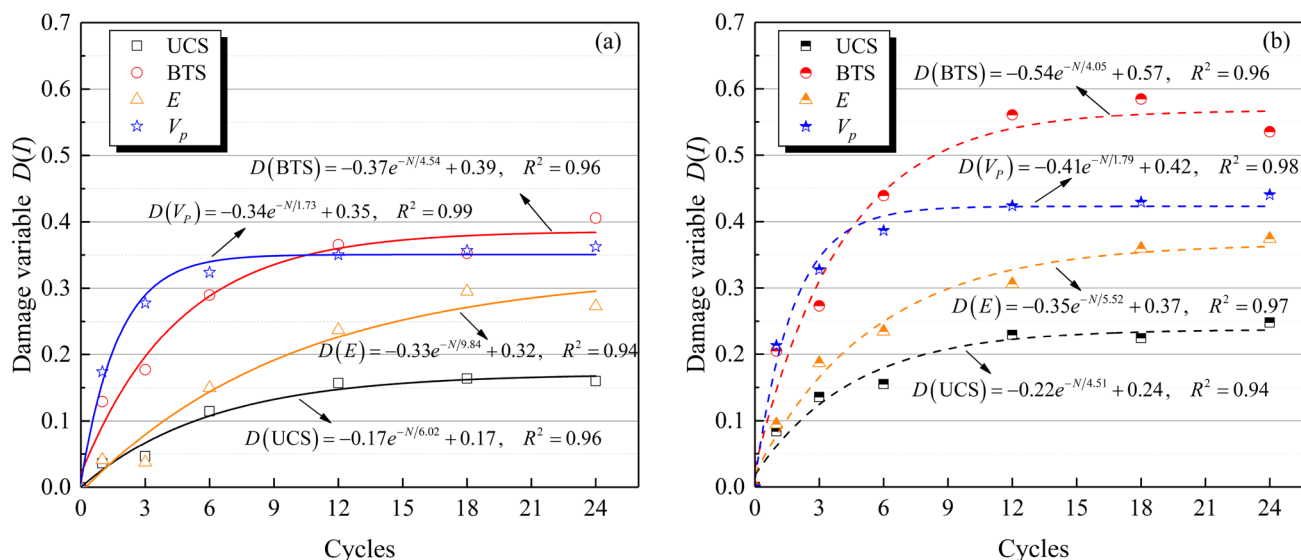


Fig. 19 Damage variables of **a** AG sample and **b** LG sample versus the number of heating-cooling cycles

fracturing should be reasonably determined based on the on-site geological conditions, construction operating costs and fracture connectivity.

In addition, it can also be considered to use the cryogenic LN_2 to assist in drilling operations, which is one of the critical processes for the exploitation of HDR geothermal energy through EGSs. As pointed by Huang and Meng (2018), the traditional drilling fluid under a relative higher temperature is difficult to perform the normal functions, such as protecting well walls and carrying cutting. According to the current experimental results, the cryogenic LN_2 can significantly reduce the threshold of crack initiation and damage stress. This is quite beneficial for reducing the broken initiation pressure of rock and improving the drilling efficiency. At present, a method of high-pressure LN_2 jet assisted drilling, which combines the double shock effect of the cryogenic LN_2 and high-speed jet, has been proposed by some researchers (Huang et al. 2015, 2019). Along with the high efficiency in breaking rock, this method is also considered to have an excellent performance in cleaning the bottom hole and carrying cuttings. Unfortunately, due to the lack of a comprehensive understanding of the influencing factors and damage mechanisms of rock breaking with LN_2 , it has not been practically used in HDR drilling operations. This will be a significant issue to investigate the fracture initiation stress and fracture characteristics of high-temperature rocks under different stress states and jet pressures in the further work.

It has to be acknowledged that there are still many fundamental and technical issues still need to be solved before the widespread adoption of the LN_2 fracturing technology. The development of a dedicated large-scale cryogenic fluid

pumping equipment is a prerequisite for on-site LN_2 fracturing. Besides that, the vaporization of LN_2 is also an obstacle that must be addressed. During the injection of LN_2 , some effective measures must be taken to keep its cryogenic state, so as to maximize the thermal shock damage to the reservoir rock. Considering the cryogenic characteristic of LN_2 , the transport pipelines should be able to maintain the original strength for a long time in an ultra-low temperature environment. In addition, it is hard for LN_2 to carry sufficient proppant into the crack due to its low viscosity (Han et al. 2018). Although some scholars suggested that the delivery efficiency of proppant can be improved by increasing the injection rate of LN_2 (Gupta and Bobier, 1998; Wang et al. 2016), it is still urgent to develop a new a new proppant suitable for carrying by LN_2 .

5 Conclusions

In this paper, the effects of cyclic LN_2 cooling and air cooling on the physico-mechanical properties of high-temperature granite are comparatively studied. The damage mechanism of LN_2 cooling cycles on high-temperature rocks and its potential engineering applications are discussed. The major conclusions can be drawn from the study include:

- (1) Irrespective of the cooling method, the increasing number of heating-cooling cycles leads to a continuous deterioration of the physico-mechanical properties of granite, manifested by the increase in porosity, and the decay of P-wave velocity, strength and deformation properties. The variation of rock properties with the

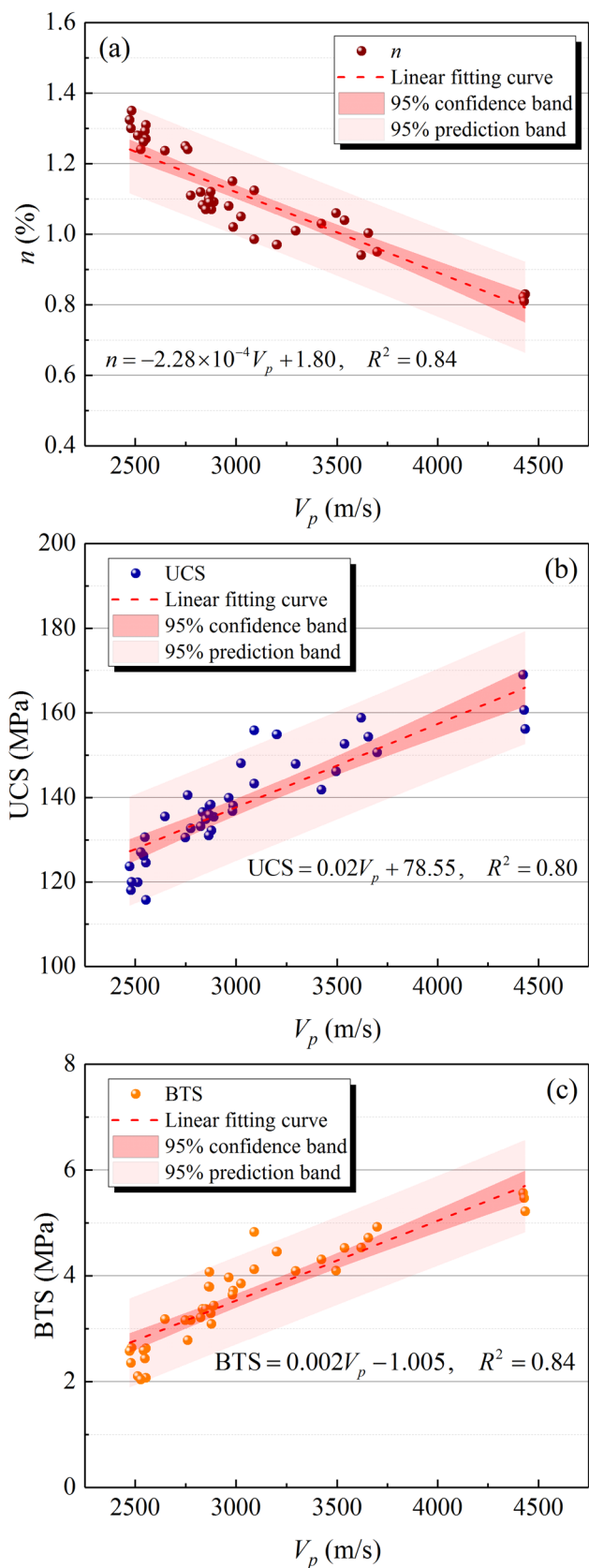


Fig. 20 Relationship between **a** n , **b** UCS, **c** BTS and V_p of granite sample

number of cycles can be well described by exponential functions.

- (2) The intense thermal shock induced by LN_2 quenching further exacerbates the degradation of the macroscopic properties of the granite compared to that with air cooling. Microscopic observations reveal that LG samples exhibits more severe microstructural damage than AG samples, as evidenced by more pronounced crack growth and larger crack widths.
- (3) The deterioration rate of physico-mechanical properties of granite gradually reduces with the increase in cycle number. After about 12 cycles, the damage to granite induced by the heating–cooling cycle is less prominent. This is attributed to the fact that the growing micro-defects provide sufficient space for thermal deformation of the minerals, thus reducing the level of thermal stress in the rock.

Acknowledgements This work was supported by the National Natural Science Foundation of China (Grant nos. 41772305 and 51579189), and Guangxi Key Research and Development Plan (Guike NO. AB18126046). These supports are gratefully acknowledged.

Compliance with ethical standards

Conflict of interest The authors declare that they have no conflict of interest.

References

Alqatahni NB, Cha MS, Yao BW, Yin XL (2016) Experimental investigation of cryogenic fracturing of rock specimens under true triaxial-confining stresses. SPE Europe featured at 78th EAGE conference and exhibition, Vienna, Austria, SPE-180071-MS

Bahrami R, Rezaee R, Clennell B (2012) Water blocking damage in hydraulically fractured tight sand gas reservoirs: an example from Perth Basin. West Aust J Pet Sci Eng 88–89(S1):100–106

Barla G (2017) Comprehensive study including testing, monitoring and thermo-hydro modelling for design and implementation of a geothermal system in Torino (Italy). Geomech Geophys Geo Energy Geo Resour 3(2):175–188

Bertani R (2005) World geothermal power generation in the period 2001–2005. Geothermics 34(6):651–690

Bieniawski ZT (1967) Mechanism of brittle fracture of rock. Int J Rock Mech Min Sci Geomech Abstr 4(4):395–430

Boudet H, Clarke C, Bugden D, Maibach E, Roser-Renouf C, Leiserowitz A (2014) “Fracking” controversy and communication: Using national survey data to understand public perceptions of hydraulic fracturing. Energy Policy 65:57–67

Brace WF, Paulding BW, Scholz CH (1966) Dilatancy in the fracture of crystalline rocks. J Geophys Res 71(16):3939–3953

Brannon HD (2010) Hydraulic fracturing materials: application trends and consideration. In: Proceedings of SPE Distinguished Lecture Program Society of Petroleum Engineers Richardson TX

Breede K, Dzebisashvili K, Liu XL, Falcone G (2013) A systematic review of enhanced (or engineered) geothermal systems: past, present and future. Geotherm Energy 1(1):4

- Cai M, Kaiser PK, Tasaka Y, Maejima T, Morioka H, Minami M (2004) Generalized crack initiation and crack damage stress thresholds of brittle rock masses near underground excavations. *Int J Rock Mech Min Sci* 41(5):833–847
- Cai CZ, Li GS, Huang ZW, Shen ZH, Tian SC (2014a) Rock pre structure damage due to freeze during liquid nitrogen fracturing. *Arab J Sci Eng* 39(12):9249–9257
- Cai CZ, Li GS, Huang ZW, Shen ZH, Tian SC, Wei JW (2014b) Experimental study of the effect of liquid nitrogen cooling on rock pore structure. *J Nat Gas Sci Eng* 21:507–517
- Cai CZ, Li GS, Huang ZW, Tian SC, Shen ZH, Fu X (2015) Experiment of coal damage due to super-cooling with liquid nitrogen. *J Nat Gas Sci Eng* 22:42–48
- Cai CZ, Huang ZW, Li GS, Gao F, Wei JW, Li R (2016) Feasibility of reservoir fracturing stimulation with liquid nitrogen jet. *J Petrol Sci Eng* 144:59–65
- Cha MS, Alqahtani NB, Yin XL, Kneafsey TJ, Bowen Yao WuYS (2017) Laboratory system for studying cryogenic thermal rock fracturing for well stimulation. *J Petrol Sci Eng* 156:780–789
- Chaki S, Takarli M, Agbodjan WP (2008) Influence of thermal damage on physical properties of a granite rock: porosity, permeability and ultrasonic wave evolutions. *Constr Build Mater* 22(7):1456–1461
- Dwivedi RD, Goela RK, Prasada VVR, Sinha A (2008) Thermo-mechanical properties of Indian and other granites. *Int J Rock Mech Min Sci* 45(3):303–315
- Eberhardt E, Stead D, Stimpson B, Read RS (1998) Identifying crack initiation and propagation thresholds in brittle rock. *Can Geotech J* 35(2):222–233
- Elwegaa K, Emadi H (2018) The effect of thermal shocking with nitrogen gas on the porosities, permeabilities, and rock mechanical properties of unconventional reservoirs. *Energies* 11(8):1–16
- Finnie I, Cooper GA, Berlie J (1979) Fracture propagation in rock by transient cooling. *Int J Rock Mech Min Sci Geomech Abstr* 16(1):11–21
- Fredrich JT, Wong TF (1986) Micromechanics of thermally induced cracking in three crustal rocks. *J Geophys Res* 91(B12):12743–12764
- Gallup DL (2009) Production engineering in geothermal technology: A review. *Geothermics* 38(3):326–334
- Gao F, Cai CZ, Yang YG (2018) Experimental research on rock fracture failure characteristics under liquid nitrogen cooling conditions. *Results Phys* 9:252–262
- Grundmann SR, Rodvelt GD, Dials GA, Allen RE (1998) Cryogenic nitrogen as a hydraulic fracturing fluid in the Devonian shale, Society of Petroleum Engineers. SPE, Pittsburgh, p 51067
- Gupta DV, Bobier DM (1998) The history and success of liquid CO₂ and CO₂/N₂ fracturing system. In: SPE Gas Technology Symposium, Society of Petroleum Engineers SPE 40016
- Hall K (1999) The role of thermal stress fatigue in the breakdown of rock in cold regions. *Geomorphology* 31(1–4):47–63
- Han SC, Cheng YF, Gao Q, Yan CL, Han ZY (2018) Experimental study of the effect of liquid nitrogen pretreatment on shale fracability. *J Nat Gas Sci Eng* 60:11–23
- Hardy HR (1994) Geotechnical field applications of AE/MS techniques at the Pennsylvania state university: a historical review. *NDT E Int* 27(4):191–200
- Homandtienne F, Troalen JP (1984) Behavior of granites and limestones subjected to slow and homogeneous temperature changes. *Eng Geol* 20(3):219–233
- Hu JJ, Sun Q, Pan XH (2018) Variation of mechanical properties of granite after high-temperature treatment. *Arab J Geosci* 11(2):43
- Huang XQ, Meng QK (2018) Feasibility study on application of liquid nitrogen in hot dry rock drilling. *Explor Eng (Rock Soil Drill Tunn)* 45(2):22–25
- Huang ZW, Li GS, Cai CZ, Wei JW (2015) Experiment of liquid nitrogen cryogenic cracking on rock and its application prospect in oil & gas exploration and production. *J Northeast Univ (Nat Sci)* 36(S1):158–162
- Huang ZW, Wu XG, Li ZSK, Yang RY (2019) Mechanism of drilling rate improvement using high-pressure liquid nitrogen jet. *Petrol Explor Dev* 46(4):768–775
- Hueckel T, Peano A, Pellegrini R (1994) A constitutive law for thermo-plastic behaviour of rocks: an analogy with clays. *Surv Geophys* 15(5):643–671
- Inada Y, Yokota K (1984) Some studies of low temperature rock strength. *Int J Rock Mech Min Sci Geomech Abstr* 21(3):145–153
- Jackson RE, Gorody AW, Mayer B, Roy JW, Ryan MC, Van Stempvoort DR (2013) Groundwater protection and unconventional gas extraction: the critical need for field-based hydrogeological research. *Ground Water* 51:488–510
- Jacobsen RT, Stewart RB, Jahangiri M (1986) Thermodynamic properties of nitrogen from the freezing line to 2000 K at pressures to 1000 MPa. *J Phys Chem* 15(2):735–909
- Kim K, Kemeny J, Nickerson M (2013) Effect of rapid thermal cooling on mechanical rock properties. *Rock Mech Rock Eng* 47(6):2005–2019
- Kim JS, Lee KS, Cho WJ, Choi HJ, Cho GC (2015) A comparative evaluation of stress–strain and acoustic emission methods for quantitative damage assessments of brittle rock. *Rock Mech Rock Eng* 48(2):495–508
- Kranz RL (1983) Microcracks in rocks: a review. *Tectonophysics* 100(1):449–480
- Kumari WGP, Ranjith PG, Perera MSA, Chen BK, Abdulagatov IM (2017) Temperature-dependent mechanical behaviour of Australian Strathbogie granite with different cooling treatments. *Eng Geol* 229:31–44
- Li ZF, Xu HF, Zhang CY (2016) Liquid nitrogen gasification fracturing technology for shale gas development. *J Petrol Sci Eng* 138:253–256
- Mansurov VA (1994) Acoustic emission from failing rock behaviour. *Rock Mech Rock Eng* 27(3):173–182
- Martin CD, Chandler NA (1994) The progressive fracture of Lac du Bonnet granite. *Int J Rock Mech Min Sci Geomech Abstr* 31(6):643–659
- McDaniel B, Grundmann SR, Kendrick WD, Wilson DR, Jordan SW (1997) Field applications of cryogenic nitrogen as a hydraulic-fracturing fluid. SEP Annual Technical Conference and Exhibition, Society of Petroleum Engineers, Texas, p 38623
- Nicksiar M, Martin CD (2012) Evaluation of methods for determining crack initiation in compression tests on low-porosity rocks. *Rock Mech Rock Eng* 45(4):607–617
- Olasolo P, Juarez MC, Olasolo J, Morales MP, Valdani D (2016) Economic analysis of Enhanced Geothermal Systems (EGS). A review of software packages for estimating and simulating costs. *Appl Therm Eng* 104:647–658
- Peng J, Yang SQ (2018) Comparison of mechanical behavior and acoustic emission characteristics of three thermally-damaged rocks. *Energies* 11(9):2350
- Peng J, Rong G, Cai M, Zhou CB (2015) A model for characterizing crack closure effect of rocks. *Eng Geol* 189:48–57
- Peng J, Rong G, Yao MD, Wong LNY, Tang ZC (2018) Acoustic emission characteristics of a fine-grained marble with different thermal damages and specimen sizes. *B Eng Geol Environ* 78(6):4479–4491
- Perras MA, Diederichs MS (2014) A review of the tensile strength of rock: concepts and testing. *Geotech Geol Eng* 32(2):525–546
- Potter RM, Robinson ES, Smith MC (1974) Method of extracting heat from dry geothermal reservoirs. US Patent No.3786858, USA, Los Alamos, New Mexico.
- Qin L, Zhai C, Liu SM, Xu JZ, Tang ZQ, Yu GQ (2016) Failure mechanism of coal after cryogenic freezing with cyclic liquid nitrogen

- and its influences on coalbed methane exploitation. *Energy Fuels* 30(10):8567–8578
- Qin L, Zhai C, Liu SM, Xu JZ, Yu GQ, Sun Y (2017) Changes in the petrophysical properties of coal subjected to liquid nitrogen freeze-thaw—A nuclear magnetic resonance investigation. *Fuel* 194:102–114
- Qin L, Zhai C, Liu SM, Xu JZ (2018a) Infrared thermal image and heat transfer characteristics of coal injected with liquid nitrogen under triaxial loading for coalbed methane recovery. *Int J Heat Mass Tran* 118:1231–1242
- Qin L, Zhai C, Liu SM, Xu JZ (2018b) Mechanical behavior and fracture spatial propagation of coal injected with liquid nitrogen under triaxial stress applied for coalbed methane recovery. *Eng Geol* 233:1–10
- Qin Y, Tian H, Xu NX, Chen Y (2020) Physical and mechanical properties of granite after high-temperature treatment. *Rock Mech Rock Eng* 53(1):305–322
- Reuschlé T, Gbaguidi Haore S, Darot M (2006) The effect of heating on the microstructural evolution of la peyrate granite deduced from acoustic velocity measurements. *Earth Planet Sci Lett* 243(3–4):692–700
- Rong G, Yao MD, Peng J, Sha S, Tan J (2018) Influence of initial thermal cracking on physical and mechanical behaviour of a coarse marble: insights from uniaxial compression tests with acoustic emission monitoring. *Geophys J Int* 214(3):1886–1900
- Rybach L (2014) Geothermal power growth 1995–2013—a comparison with other renewables. *Energies* 7(8):4802–4812
- Sha S, Rong G, Peng J, Li BW, Wu ZJ (2019) Effect of open-fire-induced damage on Brazilian tensile strength and microstructure of granite. *Rock Mech Rock Eng* 52(11):4189–4202
- Shao SS, Wasantha PLP, Ranjith PG, Chen BK (2014) Effect of cooling rate on the mechanical behavior of heated Strathbogie granite with different grain sizes. *Int J Rock Mech Min Sci* 70:381–387
- Shouldice SP (1964) Liquid nitrogen developments and applications in drilling and completion operations. *J Can Petrol Technol* 3(4):158–164
- Simmons G, Cooper HW (1978) Thermal cycling cracks in three igneous rocks. *Int J Rock Mech Min Sci Geomech Abst* 15(4):145–148
- Sinal ML, Lancaster G (1987) Liquid CO₂ fracturing: advantages and limitations. *J Can Petrol Technol* 26(5):26–30
- Siratovich PA, Heap MJ, Villeneuve MC, Cole JW, Kennedy BM, Davidson J, Reuschlé T (2016) Mechanical behaviour of the rotokawa andesites (new zealand): insight into permeability evolution and stress-induced behaviour in an actively utilized geothermal reservoir. *Geothermics* 64:163–179
- Sirdesa NN, Singh TN, Ranjith PG, Singh R (2017) Effect of varied durations of thermal treatment on the tensile strength of red sandstone. *Rock Mech Rock Eng* 50(1):205–213
- Sun Q, Zhang W, Xue L, Zhang Z, Su T (2015) Thermal damage pattern and thresholds of granite. *Environ Earth Sci* 74(3):2341–2349
- Ulusay R, Hudson JA (2007) The complete ISRM suggested methods for rock characterization, testing and monitoring: 1974–2006. ISRM Commission on Testing Methods, Ankara
- Vidal J, Genter A (2018) Overview of naturally permeable fractured reservoirs in the central and southern upper rhine graben: insights from geothermal wells. *Geothermics* 74:57–73
- Wang L, Yao BW, Cha MS, Alqahtani NB, Patterson TW, Kneafsey TJ, Miskimins JL, Yin XL, Wu YS (2016) Waterless fracturing technologies for unconventional reservoirs—opportunities for liquid nitrogen. *J Nat Gas Sci Eng* 35:160–174
- Wong TF, Brace W (1979) Thermal expansion of rocks: some measurements at high pressure. *Tectonophysics* 57(2–4):95–117
- Wu XG, Huang ZW, Li R, Zhang SK, Wen HT, Huang PP, Dai XW, Zhang CC (2018) Investigation on the damage of high-temperature shale subjected to liquid nitrogen cooling. *J Nat Gas Sci Eng* 57:284–294
- Wu XG, Huang ZW, Zhao HQ, Zhang SK (2019) A transient fluid-thermo-structural coupling study of high-velocity LN₂ jet impingement on rocks. *Int J Rock Mech Min Sci* 123:UNSP 104061
- Wyborn D, Graaf L, Davidson S, Hann S (2005) Development of Australia's first hot fractured rock (HFR) underground heat exchanger, Cooper Basin, South Australia. In: *Proceedings of the world geothermal congress, Antalya, 24–29 April 2005*.
- Yang SQ, Ranjitha PG, Jinga HW, Tiana WL, Ju Y (2017a) An experimental investigation on thermal damage and failure mechanical behavior of granite after exposure to different high temperature treatments. *Geothermics* 65:180–197
- Yang ZZ, Zhang YP, Jia M, Li XG, Wei Z, Zhang L (2017b) Experimental research on influence of low temperature on coal permeability. *Rock Soil Mech* 38(2):354–359
- Yavuz H, Demirdag S, Caran S (2010) Thermal effect on the physical properties of carbonate rocks. *Int J Rock Mech Min Sci* 47(1):94–103
- Zhang CD, Liang WG, Li ZG, Xu SG, Zhao YS (2015) Observations of acoustic emission of three salt rocks under uniaxial compression. *Int J Rock Mech Min Sci* 77:19–26
- Zhang WQ, Sun Q, Hao SQ, Geng JS, Lü C (2016) Experimental study on the variation of physical and mechanical properties of rock after high temperature treatment. *Appl Therm Eng* 98:1297–1304
- Zhao XG, Cai M, Wang J, Ma LK (2013) Damage stress and acoustic emission characteristics of the Beishan granite. *Int J Rock Mech Min Sci* 64(12):258–269

Publisher's Note Springer Nature remains neutral with regard to jurisdictional claims in published maps and institutional affiliations.